



Universiteit Utrecht

INSTITUTE FOR THEORETICAL PHYSICS
MATHEMATICAL INSTITUTE

The Fokker-Planck Equation for Active Matter

Author:

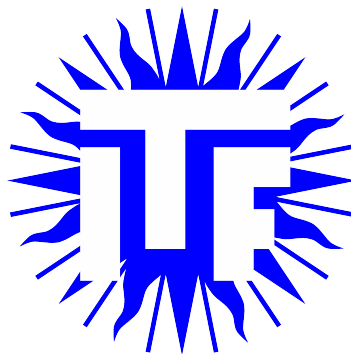
RENS PIETER DE HAAS

Supervisors:

PROF. DR. R.H.H.G. VAN ROIJ

PROF. DR. IR. J.E. FRANK

A.J. RODENBURG M.Sc.



June 2017

This page has been intentionally left blank

Acknowledgements

At first, I would like to thank my daily supervisor Jeroen Rodenburg. His door was always open if I had any questions or remarks. He showed a great interest in my progress including all my preliminary derivations. In this way, Jeroen gave me the opportunity to have detailed discussions. Those discussions often helped me when I got stuck. Sometimes Jeroen helped me by making own derivations.

My supervisors Prof. Dr. René van Roij and Prof. Dr. Ir. Jason Frank gave me the opportunity to work with them. I thank René for allowing me in his research group and providing me with this suitable research topic. I thank Jason for being willing to supervise me in a field other than his own specialization. He was able to offer a valuable different point of view to the problems.

This page has been intentionally left blank

Abstract

Active particles swim by themselves and are not in equilibrium on a local scale. We characterize the self propulsion speed with the dimensionless Peclet number $Pe = \sqrt{3}v_0/\sqrt{D_t D_r}$, which is the relative importance of the self propulsion speed v_0 with respect to the translational and rotational diffusion with diffusion coefficients D_t and D_r respectively. In this thesis we consider N identical active Brownian particles in a viscous fluid such that their motion is overdamped and given by the Langevin equations. We assume that the interaction potential between the particles is isotropic.

We derive the corresponding Fokker-Planck equation. From here we derive a hierarchy similar to the so-called BBGKY hierarchy, which is an equation for a n -particle distribution function in terms of the $(n + 1)$ -particle distribution function forming a coupled chain of equations. To obtain numerical stability, we derive in the equation for the density that the repulsions can be viewed as an excluded volume contribution and an additional term for an anisotropic correlation function. We show that this equation agrees with density functional theory in equilibrium.

If we assume no correlations and a Van der Waals fluid without self propulsion, we find numerical agreement with the normal gas-liquid binodal obtained from the conditions of equal temperature, chemical potential and pressure. When we include a small self propulsion speed to this model, we find the critical temperature decreases.

We show in a stability analysis that it is unlikely to find spontaneous motility induced phase separation (MIPS), if we assume the correlation function to be isotropic.

For active particles with a potential that is isotropic, the correlation function is found to be anisotropic. In the low-density limit in two dimensions, we were able to calculate the 2-particle correlation function. We demonstrated this for a Weeks-Chandler-Anderson (WCA) potential. We show that our results obtained from the numerical evaluation of the F-P equation agree with results of simulating the equations of motion of 1020 particles. Our results are far more accurate; we were able to determine the asymptotic decay. For low self propulsion speeds ($Pe < 1$), we derived the correlation length to be $\xi_0 = \sqrt{2D_t/D_r} = \sqrt{2/3}\sigma$ where σ is the particle diameter and the numerical results agree with this analytic result.

For ideal active particles near a (hard) wall with low self propulsion speeds ($Pe < 1$), we derived the correlation length to be $\xi = \sqrt{D_t/D_r} = \sqrt{1/3}\sigma$. Numerical calculations agree with this analytic result.

We conclude that the correlation length corresponding to the correlation function of two active particles deviates by a factor $\sqrt{2}$ of the correlation length corresponding to an active particle near a wall. This deviates from the universal correlation length in equilibrium without self propulsion as shown by Carvalho and Evans (1994) using a pole structure analysis. We can explain our factor $\sqrt{2}$. However, we did not compare our derivation from the F-P equation with their pole analysis.

Table of contents

List of figures	ix
List of tables	xiii
1 Introduction	1
1.1 Active Matter	1
1.2 Phase Coexistence	2
1.3 The Two-Body Correlation Function	5
1.4 Outline	7
2 The Fokker-Planck Equation	9
2.1 The Equations of Motion	9
2.2 The Fokker-Planck Equation for all N Particles	11
2.3 Reduction of the Phase Space to the n -Particle Distribution Function .	12
2.4 The 1-Particle Density Function	13
2.5 The Closure: The Two-Body Correlation Function	15
3 Analytic Expression for the Correlation Length	17
3.1 General Expression for the Correlation Function at Distances Larger than the Range of the Force	17
3.2 One Particle Near a Wall	22
4 Stability Analysis of a Homogeneous Density	23
4.1 Isotropic Correlation Function	23
4.2 Unstable or Stable Perturbations to a Homogeneous Density	25
4.3 MIPS with Isotropic Correlation Function	26
4.4 Considering the Force in the Stability Analysis	27
4.5 The Stability Analysis Without the Excluded Volume Approximation .	28
4.6 Stability Analysis of a Van der Waals Gas in Equilibrium	29

4.7	Stability Analysis of a Van der Waals Theory out of Equilibrium	30
5	Numerical Results	31
5.1	The Correlation Length of Ideal Particles Near a Wall	31
5.2	The Pair Correlation Function $g_{\rho=0}^{(2)}$ in 2D	34
5.3	The Correlation Length of the Correlation Function	35
5.4	Liquid-Gas Phase Coexistence in 2D	38
6	Conclusion	41
6.1	The Correlation Lengths is not Universal	41
6.2	Proof of Concept to find Phase Separation	42
7	Outlook	43
7.1	With the F-P approach	43
7.2	Different Approaches Required	44
	References	47
	Appendix A Derivations to obtain the Fokker-Planck Equation	49
A.1	The Fokker-Planck Equation	49
A.2	The Reduced Phase Space of the Fokker-Planck Equation	50
A.3	Van der Waals Free Energy to the Fokker-Planck Equation in Equilibrium	52
A.4	The Fokker-Planck and the Excluded Volume Contribution for the Density	53
A.5	Translational Invariance in the Two Body Correlation Function	56
A.6	Rotational Invariance in 2D at Low Densities	57
	Appendix B Numerics	59
B.1	Finite Element Methods	59
B.2	Initial Value Problem	62
	Appendix C Addendum: The Correlation Length Beyond the Low Self Propulsion Speed Limit	65
C.1	Analytical Expression for the One Particle Distribution Function away from a Wall	65
C.2	The Correlation Length of an Ideal Gas Near a Wall	67
C.3	The Correlation Length of the Correlation Function	68

List of figures

1.1	We show an intuitive illustration of the destruction of the normal liquid-gas coexistence for active particles. The particles have short ranged repulsions and long ranged attractions. We observe 6 particles in the liquid phase and two in the gas phase. Particles in the interface point towards the low density phase; they cannot swim away as long as the attractions are stronger than the self propulsion. Particles in the interface pointing towards the high density phase will (slowly) swim towards the center.	3
1.2	We show an intuitive illustration of the forming of MIPS. The particles are purely repulsive, there are no attractions. We see 6 particles ‘stick’ together and form a high density phase, while two particles are in the low density phase. Particles in the interface point towards the high density phase, otherwise they swim away instantaneously.	4
1.3	Illustration of the correlation function of passive particles and active particles at low and high density. The arrows represent the orientation of the particles.	6
2.1	Illustration of the particles and the coordinate system. The solid arrows within the particles indicate the direction of the self propulsive force. The gray points represent the solvent molecules.	10
2.2	Illustration of splitting the pair potential up in a short ranged and long ranged part. We will derive the short ranged interactions as an excluded volume.	13
2.3	Illustration of the relative coordinate system in 2 dimensions. The arrows within the particles indicate the direction of the self propulsive force.	16

5.1	Shown are the density and polarization profile in equilibrium ($Pe = 0$) and for an active fluid ($Pe = 1$).	31
5.2	The density profile for an active 2-dimensional ideal particles near a hard wall is shown with Peclet number $Pe = 1$. Different lines represent different orientations.	32
5.3	Shown is the decay of the densities and polarizations of an ideal 2-dimensional active gas near a hard wall for different Peclet numbers. The Peclet numbers 0.01 (brown), 0.03 (dark red), 0.1 (red), 0.3 (orange), 1 (yellow), 3 (cyan), 10 (blue), 30 (purple) and 100 (pink) are shown. The dashed black lines are fits of an exponential $A \exp[-x/\xi]$ with ξ the correlation length and A the amplitude.	33
5.4	The correlation lengths and amplitudes obtained from the fit of particles near a wall is illustrated as a function of Peclet number. These are shown for the densities (blue crosses \times) and for the polarizations (red plus $+$).	33
5.5	The two-body correlation function $g_{\theta_1, \theta_2}^{(2)}(r)$ as a function of distance for fixed orientations. A WCA potential with $\beta\epsilon = 3$ is used. The lines are obtained from the Fokker-Planck equation, the points are obtained from simulating the EOMs of 1020 particles at a density $\rho\sigma^2 = 0.01$. The simulations were done by Siddharth Paliwal. In blue the particles point towards each other, in green the particles are parallel and in red the particles point away from each other. In the inset a zoomed image is shown.	34
5.6	The two-body correlation function $g_r^{(2)}(\theta_1, \theta_2)$ is shown as a function of the orientations for fixed distances. Again a WCA potential with $\beta\epsilon = 3$ and Peclet number $Pe = 1$ is used. It is likely to find particles close together that are pointing towards each other. The dashed lines represent the periodic boundaries of the orientations.	35
5.7	The pair correlation function is shown for different orientations and different Fourier modes, as a function of distance r for different Peclet numbers Pe . All figures represent the zero density limit for particles in a WCA potential with $\beta\epsilon = 3$. The points are the result of numerical evaluation of the F-P equation. Different colors represent different orientations (on the left in Figure a, c or e) or different Fourier modes (on the right in Figure b, d or f). The solid yellow lines are a fit of the data in that range, and the dashed yellow lines are extrapolations. . .	36

- 5.8 The maximum correlation length ξ_0 is shown in the plot. The dashed line is the analytic value $\xi_0 = \sqrt{2/3}\sigma$ in terms of the particle diameter σ , where a factor $\sqrt{1/3}$ is trivial due to the choice of units. The points are obtained from fitting the analytic function, which we fitted to the data of the F-P equation. For the small self propulsion speeds, there is agreement with the analytic value as well as a small uncertainty. 38
- 5.9 In this figure the obtained gas and liquid densities are shown. The red points are obtained from density profiles in equilibrium with $Pe = 0$ and the blue points at a self propulsion speed $Pe = 1$. The black solid line is obtained from minimizing the free energy, that is exact in the Van der Waals theory. The dotted lines are the spinodal densities obtained from the stability analysis in equilibrium. The black point is the analytically obtained critical temperature and critical density. The dashed vertical line at $\rho/\rho_c = 3$ is the maximum density allowed; otherwise the excluded volume becomes larger than the volume available. The dashed line through the blue points is a guide to the eye. 39
- B.1 Visual illustrations for finite element method. 61
- C.1 In this figure the orientation dependent part is of the one particle distribution function $\psi_{x=X}^{(1)}(\theta) \sim B(\theta)$ of an ideal gas far from a wall, is shown at large distance X for different Peclet numbers. The blue points are obtained from evaluation of the F-P equation, the red line is obtained from the analytic expression. 67
- C.2 The correlation length is shown as a function of Peclet numbers for an ideal gas near a wall. This figure is modified from Figure 5.4a. The main difference is that the correlation length $\xi_{Pe=100}$, obtained from the evaluated F-P equation, was recalculated and an analytical obtained correlation length is included (solid line). We obtained from the evaluated F-P equation the correlation length from both the density (blue crosses \times) as from the polarizations (red plus $+$). 68

-
- C.3 The correlation length for the two body distribution function is shown as a function of Peclet numbers. This figure is modified from Figure 5.8. We have included the analytical expression for the correlation length $\xi_0 = \sqrt{2}\xi$ obtained from the ideal gas near a wall (solid line). We don't have any analytical justification for the correlation length of the correlation function beyond the $Pe \rightarrow 0$ limit. The points were obtained from the numerical evaluated F-P equation. 69

List of tables

A.1	An overview of higher Virial coefficients of hard spheres in terms of the second Virial coefficient. The coefficient are taken from [3].	56
-----	--	----

This page has been intentionally left blank

Chapter 1

Introduction

1.1 Active Matter

This thesis is about the statistical physics of active matter systems. These systems contain many (colloidal) particles in a viscous fluid. We call a system active when the particles have some kind of self propulsion; the particles swim by themselves. An intuitive example is a system of bacteria with a tail used to swim. Another example is a system of colloidal Janus particles; these are colloidal spherical particles with some coating on one hemisphere that acts as a catalyst for a chemical reaction and gives rise to a force. Systems of living animals like schools of fish, flocks of birds or ant colonies, can also be considered active. Active systems are not in equilibrium, because individual particles have some self propulsion and therefore (kinetic) energy is added¹ to the system. Thus the laws of thermodynamics derived in equilibrium are no longer valid.

In this thesis, we consider a class of systems of colloidal particles in a viscous fluid, such that their motion is overdamped; the momenta can be neglected. The particles in the systems have some self propulsive force. The origin of the self propulsion force will not be considered in this thesis. Our goal in this thesis is to find the distribution functions of the system, either the one-body distribution function in an inhomogeneous system or the two body correlation function in a homogeneous system. From this we hope to observe the gas-liquid coexistence as in equilibrium. We also hoped to find a new coexistence, so-called motility-induced phase separation (MIPS). This MIPS are caused by the self propulsion, a local high density phase occurs when particles collide and keep swimming into each other. Some work on simulations of thousands

¹Of course energy is conserved. This energy was first stored as chemical energy, but was not accessible.

of particles exists [11], in which the equations of motion are solved for the individual particles. In this thesis, the equations of motion are used to derive the Fokker-Planck equation; this equation is a continuity equation for the densities. When we find a stable inhomogeneous density profile, we have found phase separation.

In this introduction we recapitulate equilibrium results. Also, we give a qualitative description and intuitive explanation of the changes when the system becomes active.

1.2 Phase Coexistence

Matter can exist in different phases like solid, liquid or gas. Matter in equilibrium can phase separate under some conditions to minimize the Helmholtz free energy $F(N, V, T)$ as a function of the number of particles N , the volume V and the temperature T . Two examples of phase separation are ice cubes (solid) in water (liquid) and steam (gas) in contact with boiling water (liquid); different phases can coexist simultaneously. When phase coexistence occurs, the different phases have the same chemical potential μ , pressure p and temperature T , given by

$$\mu_l = \mu_g = \left(\frac{\partial F(N, V, T)}{\partial N} \right)_{N^*}, \quad p_l = p_g = - \left(\frac{\partial F(N, V, T)}{\partial V} \right)_{V^*}, \quad T_l = T_g, \quad (1.1)$$

where the subscripts denote the phase.

A Single Component Van der Waals Gas in Equilibrium

One of the simplest theories for the liquid-gas phase coexistence is due to Van der Waals. A Van der Waals gas is a fluid with both attractions and repulsions. The repulsions and attractions are treated differently; the repulsions are treated as some effective excluded volume and the attractions are treated in the mean field approximation; there are no correlations.

The Helmholtz free energy of a Van der Waals gas of N particles in a volume V at temperature T in equilibrium in D dimensions is $F_{\text{vdW}} = Nk_B T \left(\log \frac{N\Lambda^D}{V-bN} - 1 \right) - aN^2/V$, where b corresponds to the excluded volume between a pair of particles and a characterizes the attractions. From Equation 1.1 the pressure p and chemical potential μ as a function of density of a liquid $\rho = \rho_l$ or the density of a gas $\rho = \rho_g$ can be obtained as:

$$p = \frac{k_B T \rho}{1 - b\rho} - a\rho^2, \quad \mu = \frac{bk_B T \rho}{1 - b\rho} + k_B T \log \frac{\rho \Lambda^D}{1 - b\rho} - 2a\rho. \quad (1.2)$$

From the equality of pressures $p_g = p_l$ in the gas and liquid phase, we obtain

$$\rho_l = \frac{1 - b\rho_g}{2b} + \frac{\sqrt{a(1 - b\rho_g)(1 + b\rho_g)^2 - 4bk_B T}}{2b\sqrt{a}\sqrt{1 - b\rho_g}}. \quad (1.3)$$

Using this and $p_l = p_g$, we can obtain the numerical value for the gas density ρ_g and liquid density ρ_l at given T , b and as provide $T < T_c$ the critical temperature. These equations can also be solved to yield a transcendental equation for ρ_l and ρ_g as in [7]. The critical temperature and density can be determined by solving $(\frac{\partial p}{\partial \rho})_{T=T_c} = 0$ and $(\frac{\partial^2 p}{\partial \rho^2})_{T=T_c} = 0$, which results [14, Eq 4.68] in

$$\rho_c = \frac{1}{3b}, \quad k_B T_c = \frac{8a}{27b}. \quad (1.4)$$

Above the critical temperature, the system will not separate in a low density phase and a high density phase. We name this a fluid phase; the gas cannot be distinguished from the liquid. Note that $T_c = 0$ in absence of any attractions, $a = 0$. This implies that any finite T satisfies $T > T_c$ and hence no gas-liquid phase coexistence is possible in absence of attractions.

Effects of Activity in Phase Coexistence

Phase separation has been observed in simulations the equations of motion (EOM) for individual particles, for example in [11]; here the EOM are solved for thousands of active particles. This has been done in equilibrium and also in active matter systems. Two features arise in active matter systems compared to matter in equilibrium.

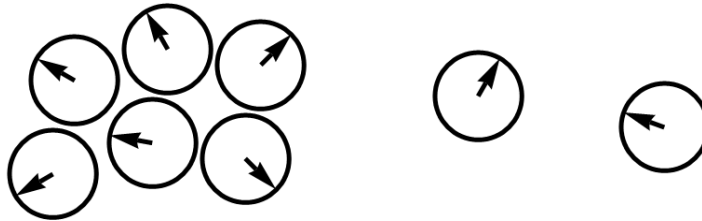


Fig. 1.1 We show an intuitive illustration of the destruction of the normal liquid-gas coexistence for active particles. The particles have short ranged repulsions and long ranged attractions. We observe 6 particles in the liquid phase and two in the gas phase. Particles in the interface point towards the low density phase; they cannot swim away as long as the attractions are stronger than the self propulsion. Particles in the interface pointing towards the high density phase will (slowly) swim towards the center.

The first feature is that in an active matter system with a gas-liquid coexistence, the critical temperature decreases and the density difference between the gas and liquid reduces or even vanishes [12]; the gas-liquid coexistence can break down into a homogeneous fluid phase. This breakdown can happen when the self propulsion is large enough compared to the attractions; the self propulsion rips the liquid phase apart. The self propulsion increases effectively the (kinetic) energy per active particle; this can be interpreted as an effective increase in temperature. An illustration of this liquid-gas coexistence is given in Figure 1.1, where particles on the interface point away from the high density phase; particles pointing towards the high density phase will swim (slowly) to the center, while particles pointing towards the low density phase cannot swim away as long as the attractions are stronger than the self propulsion. The breakdown of the phase coexistence occurs when the self propulsions are stronger than the attractions.

The second feature is that in an active matter system without any attractions, phase separation can be observed [12],[11]. A similar system without self propulsion in equilibrium does not phase separate. This new phase coexistence even occurs when the active particles only have repulsions. This phase separation can be explained by the ‘sticking’ of particles that swim towards each other. Particles collide and pile up; they cannot move away due to their self propulsion. The particles are unable to pass through each other. The density becomes non uniform and this phase separation is called motility-induced phase separation (MIPS). An illustration of this MIPS is given in Figure 1.2, where particles on the interface point towards the high density phase; particles that point away from the high density phase swim away instantly, while particles pointing towards the high density phase are blocked by other particles.

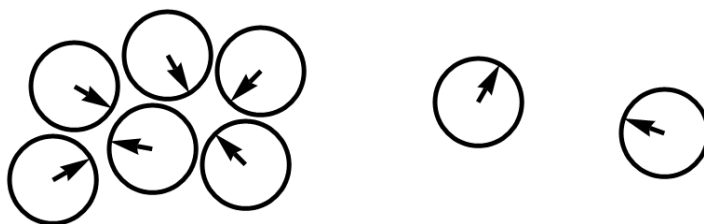


Fig. 1.2 We show an intuitive illustration of the forming of MIPS. The particles are purely repulsive, there are no attractions. We see 6 particles ‘stick’ together and form a high density phase, while two particles are in the low density phase. Particles in the interface point towards the high density phase, otherwise they swim away instantaneously.

Although the density profile of MIPS (Figure 1.2) is similar to the normal gas-liquid phase separation (Figure 1.1), the polarization and the mechanism are completely

different. We need to include the orientations in the density profile. We introduce the one-particle distribution function $\psi^{(1)}(\mathbf{r}, \boldsymbol{\theta})$ as a function of position vector \mathbf{r} and orientation vector of angles $\boldsymbol{\theta}$, where we defined the orientation of a particle by the direction of the self propulsion, not necessarily the direction of motion. The total density distribution is obtained from $\psi^{(1)}$ if we integrate the orientation dependence, i.e.

$$\rho(\mathbf{r}) = \int d\boldsymbol{\theta} \psi^{(1)}(\mathbf{r}, \boldsymbol{\theta}), \quad (1.5)$$

and the polarization is defined as

$$P_k(\mathbf{r}) = \frac{\int d\boldsymbol{\theta} \psi^{(1)}(\mathbf{r}, \boldsymbol{\theta}) \cos \theta_k}{\rho(\mathbf{r})}, \quad (1.6)$$

where θ_k is the projection of the orientation angle to the k^{th} Cartesian component. In two dimensions near a wall we only consider $P(\mathbf{r}) = P_1(\mathbf{r})$, $\theta_1 = \theta$ and possibly $\theta_2 = \theta + \pi/2$.

1.3 The Two-Body Correlation Function

One of the forces on interacting particles is the two-body force; the force between two particles. In a continuum description, the two-body force becomes an internal force. The internal force is the integral over the two-body force multiplied by the two-body distribution $\psi^{(2)}(\mathbf{r}_1, \boldsymbol{\theta}_1, \mathbf{r}_2, \boldsymbol{\theta}_2, t)$. The two-body distribution function is defined as the probability of finding one particle at position \mathbf{r}_2 and orientation $\boldsymbol{\theta}_2$ and simultaneously another particle at position \mathbf{r}_1 and orientation $\boldsymbol{\theta}_1$. Normalizing $\psi^{(2)}$ with the local densities at the same positions and time t to obtain the two-body correlation function $g^{(2)}$

$$\psi^{(2)}(\mathbf{r}_1, \boldsymbol{\theta}_1, \mathbf{r}_2, \boldsymbol{\theta}_2, t) = \psi^{(1)}(\mathbf{r}_1, \boldsymbol{\theta}_1, t) \psi^{(1)}(\mathbf{r}_2, \boldsymbol{\theta}_2, t) g^{(2)}(\mathbf{r}_1, \boldsymbol{\theta}_1, \mathbf{r}_2, \boldsymbol{\theta}_2, t). \quad (1.7)$$

In a homogeneous system the two-body correlation function does not depend on the absolute position; it only depends on the distance vector $\mathbf{r}_{12} = \mathbf{r}_2 - \mathbf{r}_1$.

Without self propulsion

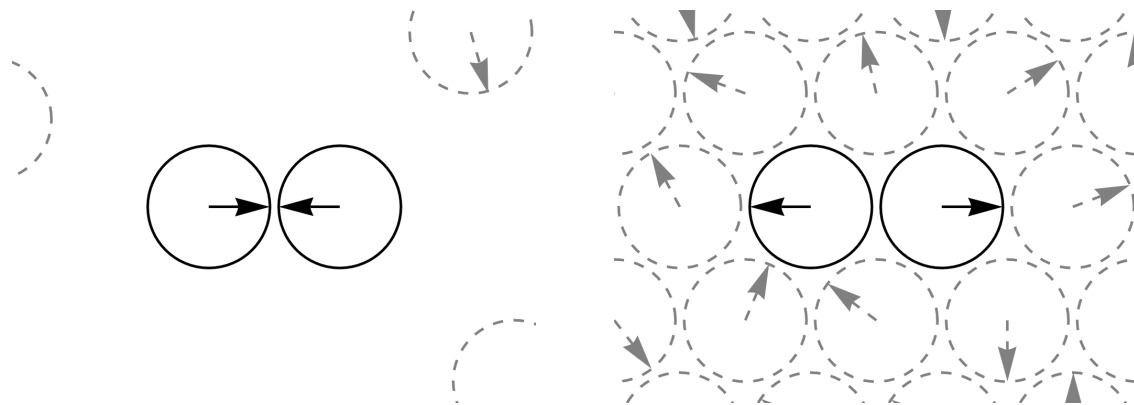
Some approximations of the two-body correlation function in equilibrium are

$$g^{(2)}(\mathbf{r}_1, \boldsymbol{\theta}_1, \mathbf{r}_2, \boldsymbol{\theta}_2) = 1 \quad \text{Mean field,} \quad (1.8a)$$

$$g^{(2)}(\mathbf{r}_1, \boldsymbol{\theta}_1, \mathbf{r}_2, \boldsymbol{\theta}_2) = \exp[-\beta\Phi_{12}(\mathbf{r}_{12})] \quad \text{Low density limit,} \quad (1.8b)$$

$$g^{(2)}(\mathbf{r}_1, \boldsymbol{\theta}_1, \mathbf{r}_2, \boldsymbol{\theta}_2) = g^{(2)}(|\mathbf{r}_{12}|) \quad \text{Isotropic fluid,} \quad (1.8c)$$

where $\Phi_{12}(\mathbf{r}_{12})$ is the two particle potential. In the mean field approximation interactions are included, though the correlations are neglected as in Equation 1.8a. A low density approximation is given in Equation 1.8b; intuitively, this approximation is the Boltzmann weight of the pair potential Φ_{12} between the two particles. This approximation includes correlations up to the 2nd Virial expansion. In a homogeneous density fluid without spontaneous symmetry breaking, the correlation function of isotropic particles only depends on the absolute distance, see Equation 1.8c.



(a) At low density, particles with self propulsion close to each other, will likely point towards each other. Particles pointing away from each other will instantaneously swim away.

(b) At high density, particles with self propulsion can point in all directions, two particles cannot swim away from each other; they are blocked by the other particles.

Fig. 1.3 Illustration of the correlation function of passive particles and active particles at low and high density. The arrows represent the orientation of the particles.

With self propulsion at low densities

At low densities, particles that swim by themselves, can ‘stick’ together, even if they are purely repulsive. This can be explained by considering two particles (very low density) that each have a self propulsion force and a repulsive force between them.

If the particles have an orientation such that the self propulsion makes them swim towards each other, they can collide. The repulsion keeps them from passing through each other while the self propulsion keeps them together; they ‘stick’ together. An illustration of this ‘sticking’ is in Figure 1.3a. Of course, due to rotational Brownian forces/diffusion, the orientation of the particles changes over time. However, this diffusion contributes on longer time scales. When they no longer point towards each other, they swim away instantaneously and no longer ‘stick’. This effect will cause the two-body correlation function to be orientation dependent. Particles close together will likely swim towards each another.

With self propulsion at high densities

The low-density effect of particles, that likely point towards each other, is damped at high densities. Consider a particle at a high density. Everywhere around this particle, there are other particles nearby as is illustrated in Figure 1.3b, independent of their orientations. A pair of particles that points away from each other cannot swim away, since other particles present block them. The orientation distribution becomes isotropic² in a bulk high density phase, caused by diffusion in the orientation phase space.

1.4 Outline

In Chapter 2 we introduce the equations of motion and we derive the Fokker-Plank equation. We also derive a hierarchy similar to the BBKGY hierarchy. The equations derived in this chapter are the base of the rest of this thesis.

In Chapter 3 the asymptotic decay of the 2-particle correlation function and 1-particle distribution function are derived from the F-P equation. For small Peclet numbers we can determine the correlation lengths. For large Peclet numbers our results are inconclusive.

In Chapter 4 we consider a perturbation to a homogeneous density distribution and determine, using the F-P equation, if there exists an unstable perturbative mode. With this we can exclude the possibility of spontaneous phase separation.

In Chapter 5 we will show the results obtained from numerical evaluations of the F-P equation. We determine the gas-liquid binodal in equilibrium and out-of-equilibrium.

²For particles with a potential that is isotropic.

We compare the correlation function to simulations, and we determine the asymptotic decay and the correlation length.

In Chapter 6 we summarize our results and draw our conclusions. The most significant conclusion is that the correlation length is no longer universal, unlike equilibrium.

In Chapter 7 we give an outlook.

In Appendix A most derivations required in Chapter 2 are presented.

In Appendix B we give a very brief introduction to finite element methods and the Rutta-Kunga method. These are methods to determine a numerical solution to a partial differential equation, which is either a boundary value problem or an initial value problem.

Chapter 2

The Fokker-Planck Equation

In this chapter the Fokker-Planck equation is derived for an overdamped system of N active particles. Starting with the equations of motion in Section 2.1, which comprise a system of stochastic differential equations (SDE), partial differential equations (PDE) for the N -particle distribution $\psi^{[N]}(\mathbf{r}^N, \boldsymbol{\theta}^N, t)$ are obtained in Section 2.2. In Section 2.3 the phase space is reduced to obtain a PDE for the n -particle distribution $\psi^{(n)}(\mathbf{r}^n, \boldsymbol{\theta}^n, t)$ for $n < N$ which depends in a hierarchical fashion on $\psi^{(n+1)}$. The PDE for the orientation dependent 1-particle distribution function $\psi^{(1)}$ is simplified in Section 2.4, which depends on the 2-particle distribution function $\psi^{(2)}$. The repulsions are treated as an excluded volume. A closure relation for $\psi^{(2)}$ is given in Section 2.5, where we use the local density approximation at low densities.

2.1 The Equations of Motion

Consider a many body problem with N active Brownian particles (ABP) that are overdamped in a solvent with positions $\{\mathbf{r}_i\}_{i \leq N}$ and orientations $\{\boldsymbol{\theta}_i\}_{i \leq N}$, as illustrated in Figure 2.1. We assume the particles have some self propulsion force, i.e. due to some chemical reaction; they swim by themselves. The orientation direction of the particle is defined as the direction of the self propulsion force, not necessarily the same as the direction of movement. We denote vectors in bold and the distance vector from particle i to particle j by $\mathbf{r}_j - \mathbf{r}_i = \mathbf{r}_{ij}$. Further, if a function depends on both the position \mathbf{r}_i as the orientation $\boldsymbol{\theta}_i$ of particle i , the shorthand notation for the argument $(\mathbf{i}) = (\mathbf{r}_i, \boldsymbol{\theta}_i)$ is used sometimes.

The class of equations of motion described in this thesis is quite general. Included are translational and rotational Brownian forces, translational and rotational drag, external forces \mathbf{F}^{ext} and torques $\boldsymbol{\Gamma}^{\text{ext}}$ and some self propulsion in the direction of

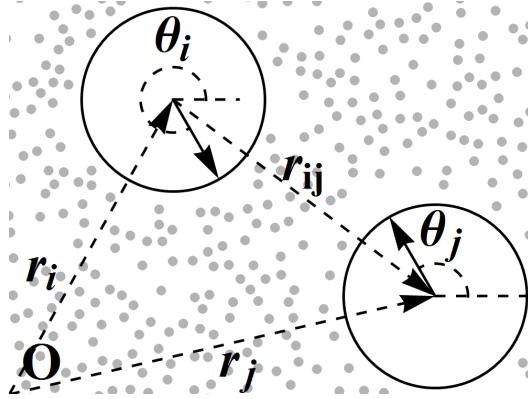


Fig. 2.1 Illustration of the particles and the coordinate system. The solid arrows within the particles indicate the direction of the self propulsive force. The gray points represent the solvent molecules.

the particle orientation with a speed v_0 . For interacting particles, internal two-body forces¹ \mathbf{F}_{ij} and two-body torques $\mathbf{\Gamma}_{ij}$ between particle i and j are also included. The interactions depend on the distance and possibly the relative orientations. Abusing notation, define $\mathbf{F}_{ij} \equiv 0$ and $\mathbf{\Gamma}_{ij} \equiv 0$ if $i = j$. The forces due to the solvent are simplified to a drag force and Brownian noise force; we do not include the full hydrodynamics of the solvent².

The equations of motion (EOM) are given by the Langevin equations. The momentum can be neglected in an overdamped system, i.e. $M \frac{\partial^2 \mathbf{r}_i}{\partial t^2} = -\gamma_t \frac{\partial \mathbf{r}_i}{\partial t} + \mathbf{F}^{\text{other}}(\mathbf{r}^N, \boldsymbol{\theta}^N)$ and $I \frac{\partial^2 \boldsymbol{\theta}_i}{\partial t^2} = -\gamma_r \frac{\partial \boldsymbol{\theta}_i}{\partial t} + \mathbf{\Gamma}^{\text{other}}(\mathbf{r}^N, \boldsymbol{\theta}^N)$, where M is the mass, I is the moment of inertia, γ_t the translational drag coefficient and γ_r rotational drag coefficients. Separating the drag term, which is the only term proportional to a first order time derivative, we

¹Later we will treat the short-ranged forces as an excluded volume and only keep the long ranged forces. A density functional theory of a Van der Waals gas will give the same result in equilibrium.

²A 3 dimensional system that is between two parallel walls where the distance between the walls is of the order of the particle size is effectively 2 dimensional. In this 2 dimensional system we can neglect the hydrodynamics, since the momentum of the solvent can leak away into these walls. The momentum of the solvent cannot leak away in a 3 dimensions bulk system without walls. We do not consider the question whether this approximation is also valid in 3 dimensions, we just assume this model without hydrodynamics.

obtain

$$\frac{\partial \mathbf{r}_i}{\partial t} = \underbrace{v_0 \mathbf{e}(\boldsymbol{\theta}_i)}_{\text{Self propulsive force}} + \underbrace{\frac{D_t}{k_B T} \mathbf{F}^{\text{ext}}(\mathbf{r}_i, \boldsymbol{\theta}_i, t)}_{\text{External force}} + \underbrace{\frac{D_t}{k_B T} \sum_j \mathbf{F}_{ij}(\mathbf{r}_{ij}, t)}_{\text{two-body force}} + \underbrace{\sqrt{2D_t} \boldsymbol{\eta}_i(t)}_{\text{Brownian}}, \quad (2.1a)$$

$$\frac{\partial \boldsymbol{\theta}_i}{\partial t} = \underbrace{\frac{D_r}{k_B T} \boldsymbol{\Gamma}^{\text{ext}}(\mathbf{r}_i, \boldsymbol{\theta}_i, t)}_{\text{External torque}} + \underbrace{\frac{D_r}{k_B T} \sum_j \boldsymbol{\Gamma}_{ij}(\mathbf{r}_{ij}, \boldsymbol{\theta}_i, \boldsymbol{\theta}_j, t)}_{\text{Internal torque}} + \underbrace{\sqrt{2D_r} \boldsymbol{\xi}_i(t)}_{\text{Brownian}}. \quad (2.1b)$$

Here k_B is the Boltzmann factor, T is the temperature. We defined the diffusion coefficients $D_t = k_B T / \gamma_t$ and $D_r = k_B T / \gamma_r$. The Brownian noises $\sqrt{2D_t} \boldsymbol{\eta}$ and $\sqrt{2D_r} \boldsymbol{\xi}$ are due to stochastic forces with a Gaussian distribution³ with zero mean and satisfying $\langle \boldsymbol{\eta}_i^{(l)}(t) \boldsymbol{\eta}_j^{(k)}(t') \rangle = \delta_{ij} \delta_{kl} \delta(t - t')$ and $\langle \boldsymbol{\xi}_i^{(l)}(t) \boldsymbol{\xi}_j^{(k)}(t') \rangle = \delta_{ij} \delta_{kl} \delta(t - t')$, with k and l denoting the Cartesian component of the vector [11].

We introduce the unit of length $x_0 = \sqrt{D_t/D_r}$, unit of time $t_0 = 1/D_r$ and unit of energy $k_B T$. To make the differential equation dimensionless we replace $t \rightarrow t/t_0$, $\mathbf{r}_j \rightarrow \mathbf{r}_j/x_0$, $\mathbf{F}^{\text{ext}} \rightarrow \frac{x_0 \mathbf{F}^{\text{ext}}}{k_B T}$, $\mathbf{F}_{ij} \rightarrow \frac{x_0 \mathbf{F}_{ij}}{k_B T}$, $\boldsymbol{\Gamma}^{\text{ext}} \rightarrow \frac{\boldsymbol{\Gamma}^{\text{ext}}}{k_B T}$ and $\boldsymbol{\Gamma}_{ij} \rightarrow \frac{\boldsymbol{\Gamma}_{ij}}{k_B T}$. We denote the dimensionless self propulsion speed by the so-called Peclet number $\text{Pe} = \sqrt{1/3} \frac{v_0 t_0}{x_0} = \sqrt{3} \frac{v_0}{\sqrt{D_t D_r}}$, such that the EOM become

$$\frac{\partial \mathbf{r}_i}{\partial t} = \sqrt{3} \text{Pe} \mathbf{e}(\boldsymbol{\theta}_i) + \mathbf{F}^{\text{ext}}(\mathbf{r}_i, \boldsymbol{\theta}_i, t) + \sum_j \mathbf{F}_{ij}(\mathbf{r}_{ij}, t) + \sqrt{2} \boldsymbol{\eta}_i(t), \quad (2.2a)$$

$$\frac{\partial \boldsymbol{\theta}_i}{\partial t} = \boldsymbol{\Gamma}^{\text{ext}}(\mathbf{r}_i, \boldsymbol{\theta}_i, t) + \sum_j \boldsymbol{\Gamma}_{ij}(\mathbf{r}_{ij}, \boldsymbol{\theta}_i, \boldsymbol{\theta}_j, t) + \sqrt{2} \boldsymbol{\xi}_i(t). \quad (2.2b)$$

2.2 The Fokker-Planck Equation for all N Particles

The EOM (2.2) give the trajectories $(\mathbf{r}_i(t), \boldsymbol{\theta}_i(t))$ in time for all particles i . The corresponding Fokker-Planck (F-P) equation is an equation which gives the evolution in time of the N -particle distribution $\psi^{(N)}$, where the N -particle distribution $\psi^{(N)}(\{\mathbf{r}_i, \boldsymbol{\theta}_i\}_{i \leq N}, t)$ gives the probability of finding N particles simultaneously at posi-

³The rotational Brownian force is small and therefore the distribution can be approximated as Gaussian.

tions $\{\mathbf{r}_i, \boldsymbol{\theta}_i\}_{i \leq N}$ at time t . The corresponding F-P equation is given by:

$$\begin{aligned} \partial_t \psi^{[N]}(\mathbf{r}^N, \boldsymbol{\theta}^N, t) = & \quad (2.3) \\ & - \sum_{j=1}^N \nabla_{\mathbf{r}_j} \cdot \left[\mathbf{v}_j(\mathbf{r}^N, \boldsymbol{\theta}^N, t) \psi^{[N]}(\mathbf{r}^N, \boldsymbol{\theta}^N, t) - D_t \nabla_{\mathbf{r}_j} \psi^{[N]}(\mathbf{r}^N, \boldsymbol{\theta}^N, t) \right] \\ & - \sum_{j=1}^N \nabla_{\boldsymbol{\theta}_j} \cdot \left[\boldsymbol{\omega}_j(\mathbf{r}^N, \boldsymbol{\theta}^N, t) \psi^{[N]}(\mathbf{r}^N, \boldsymbol{\theta}^N, t) - D_r \nabla_{\boldsymbol{\theta}_j} \psi^{[N]}(\mathbf{r}^N, \boldsymbol{\theta}^N, t) \right], \end{aligned}$$

which is essentially a continuity equation for the phase space $(\mathbf{r}^N, \boldsymbol{\theta}^N)$. Here \mathbf{v}_j and $\boldsymbol{\omega}_j$ are the drift terms in the EOM

$$\mathbf{v}_j = \sqrt{3} \text{Pe} \mathbf{e}(\boldsymbol{\theta}_i) + \mathbf{F}^{\text{ext}}(\mathbf{r}_i, \boldsymbol{\theta}_i, t) + \sum_j \mathbf{F}_{ij}(\mathbf{r}_{ij}, t), \quad (2.4a)$$

$$\boldsymbol{\omega}_j = \boldsymbol{\Gamma}^{\text{ext}}(\mathbf{r}_i, \boldsymbol{\theta}_i, t) + \sum_j \boldsymbol{\Gamma}_{ij}(\mathbf{r}_{ij}, \boldsymbol{\theta}_i, \boldsymbol{\theta}_j, t). \quad (2.4b)$$

A motivation for expressions 2.3 and 2.4 is given in Appendix A.1.

2.3 Reduction of the Phase Space to the n-Particle Distribution Function

Define the reduced phase space distribution function $\psi^{(n)}(\mathbf{r}^n, \boldsymbol{\theta}^n, t)$, which is the probability of finding n particles at positions \mathbf{r}^n with orientation $\boldsymbol{\theta}^n$ at time t . This distribution is the integral over all possible configurations of the $N - n$ other particles up to some permutation factor and is defined as

$$\psi^{(n)}(\mathbf{r}^n, \boldsymbol{\theta}^n, t) = \frac{N!}{(N-n)!} \int d\mathbf{r}^{N-n} \int d\boldsymbol{\theta}^{N-n} \psi^{[N]}(\mathbf{r}^N, \boldsymbol{\theta}^N, t). \quad (2.5)$$

Inserting Equation 2.5 into Equation 2.3 gives the time evolution of $\psi^{(n)}(\mathbf{r}^n, \boldsymbol{\theta}^n, t)$ given by

$$\begin{aligned} \frac{\partial \psi^{(n)}}{\partial t} = & - \sum_{j=1}^n \nabla_{\mathbf{r}_j} \cdot \left[\sqrt{3} \text{Pe} \mathbf{e}(\boldsymbol{\theta}_j) \psi^{(n)} + \mathbf{F}^{\text{ext}} \psi^{(n)} + \sum_{i=1}^n \mathbf{F}_{ij} \psi^{(n)} - \nabla_{\mathbf{r}_j} \psi^{(n)} \right] \\ & - \sum_{j=1}^n \nabla_{\boldsymbol{\theta}_j} \cdot \left[\Gamma^{\text{ext}} \psi^{(n)} + \sum_{i=1}^n \Gamma_{ij} \psi^{(n)} - \nabla_{\boldsymbol{\theta}_j} \psi^{(n)} \right] \\ & - \sum_{j=1}^n \nabla_{\mathbf{r}_j} \cdot \iint d\mathbf{r}_{n+1} d\boldsymbol{\theta}_{n+1} \left[\mathbf{F}_{j,n+1} \psi^{(n+1)} \right] \\ & - \sum_{j=1}^n \nabla_{\boldsymbol{\theta}_j} \cdot \iint d\mathbf{r}_{n+1} d\boldsymbol{\theta}_{n+1} \left[\Gamma_{j,n+1} \psi^{(n+1)} \right]. \end{aligned} \quad (2.6)$$

We derived this hierarchic equation in Appendix A.2. This derivation and result are similar to the Bogoliubov–Born–Green–Kirkwood–Yvon hierarchy (BBGKY hierarchy) [1]. In contrast to the standard BBGKY hierarchy, we started without momenta and included orientations.

2.4 The 1-Particle Density Function

In the case $n = 1$, denote $\mathbf{r}_1 = \mathbf{r}$ and $\boldsymbol{\theta}_1 = \boldsymbol{\theta}$, we obtain a PDE for $\psi^{(1)}(\mathbf{r}, \boldsymbol{\theta}, t)$ given by

$$\begin{aligned} \frac{\partial \psi^{(1)}}{\partial t} = & - \nabla_{\mathbf{r}} \cdot \left[\sqrt{3} \text{Pe} \mathbf{e}(\boldsymbol{\theta}) \psi^{(1)} + \mathbf{F}^{\text{ext}} \psi^{(1)} - \nabla_{\mathbf{r}} \psi^{(1)} \right] \\ & - \nabla_{\boldsymbol{\theta}} \cdot \left[\Gamma^{\text{ext}} \psi^{(1)} - \nabla_{\boldsymbol{\theta}} \psi^{(1)} \right] \\ & - \nabla_{\mathbf{r}} \cdot \iint d\mathbf{r}' d\boldsymbol{\theta}' \left[\mathbf{F}_{12} \psi^{(2)} \right] - \nabla_{\boldsymbol{\theta}} \cdot \iint d\mathbf{r}' d\boldsymbol{\theta}' \left[\Gamma_{12} \psi^{(2)} \right], \end{aligned} \quad (2.7)$$

where $F_{12} = F_{12}(\mathbf{r} - \mathbf{r}')$, $\Gamma_{12} = \Gamma_{12}(\mathbf{r} - \mathbf{r}')$ and we still need a closure relation for $\psi^{(2)} = \psi^{(2)}(\mathbf{r}, \boldsymbol{\theta}, \mathbf{r}', \boldsymbol{\theta}', t)$. A possible closure relation will be given in Section 2.5.



Fig. 2.2 Illustration of splitting the pair potential up in a short ranged and long ranged part. We will derive the short ranged interactions as an excluded volume.

The two-body force can be denoted as minus the gradient of a pair potential $\mathbf{F}_{12}(\Delta\mathbf{r}) = -\nabla\Phi_{12}(\Delta\mathbf{r})$. Split the pair potential up in $\Phi_{12} = \Phi_{12}^{\text{short}} + \Phi_{12}^{\text{long}}$ as the sum potential due to the short ranged repulsions Φ_{12}^{short} and long ranged interactions Φ_{12}^{long} , see also Figure 2.2. An excluded volume approximation can be derived to obtain a more convenient expression for $\iint d\mathbf{r}_2 d\boldsymbol{\theta}_2 \mathbf{F}_{1,2}^{\text{short}} \psi^{(2)}$. In Appendix A.3 this excluded volume approximation in equilibrium is derived in a density functional theory (DFT) framework for comparison. In Appendix A.4 a generalization for particles with self propulsion is derived from the Fokker-Planck equation. We find an effective enhancement of the diffusion due to the hard core interactions for nonzero density differences and also corrections due to the anisotropy of the correlation function. We obtain

$$\begin{aligned} \frac{\partial\psi^{(1)}}{\partial t} = & -\nabla_{\mathbf{r}} \cdot \left[\underbrace{\sqrt{3}\text{Pe}}_{\text{Self propulsion}} \underbrace{\mathbf{e}(\boldsymbol{\theta})\psi^{(1)}}_{\text{Ext. force}} + \underbrace{\mathbf{F}^{\text{ext}}\psi^{(1)}}_{\text{Ext. force}} - \underbrace{\frac{\nabla_{\mathbf{r}}\psi^{(1)}}{(1-b\rho)^2}}_{\text{Eff. enhanced diffusion}} \right] \\ & -\nabla_{\boldsymbol{\theta}} \cdot \left[\underbrace{\boldsymbol{\Gamma}^{\text{ext}}\psi^{(1)}}_{\text{Ext. torque}} - \underbrace{\nabla_{\boldsymbol{\theta}}\psi^{(1)}}_{\text{Rot. diffusion}} \right] \\ & -\nabla_{\mathbf{r}} \cdot \iint d\mathbf{r}' d\boldsymbol{\theta}' \underbrace{[\mathbf{F}_{12}^{\text{long}}\psi^{(2)}]}_{\text{Internal long-ranged forces}} - \nabla_{\boldsymbol{\theta}} \cdot \iint d\mathbf{r}' d\boldsymbol{\theta}' \underbrace{[\boldsymbol{\Gamma}_{12}\psi^{(2)}]}_{\text{Internal torques}} \\ & -\nabla_{\mathbf{r}} \cdot \psi^{(1)} \int d\boldsymbol{\theta}' \int_{B(\mathbf{r},\sigma_{HS})} d\mathbf{r}' \underbrace{\nabla_{\mathbf{r}'-\mathbf{r}} \left(\psi^{(1)}(\mathbf{r}',\boldsymbol{\theta}',t)(u^{(2)}-1) \right)}_{\text{Eff. force due to anisotropy of } g^{(2)}}, \end{aligned} \quad (2.8)$$

where $\psi^{(1)} = \psi^{(1)}(\mathbf{r}, \boldsymbol{\theta}, t)$ unless other arguments are denoted, $B(\mathbf{r}, \sigma)$ is a sphere with center \mathbf{r} and radius σ , $2b = 2B_2^{\text{HS}}$ is the excluded volume of hard spheres, $\rho(\mathbf{r}, t) = \int d\boldsymbol{\theta}' \psi^{(1)}(\mathbf{r}, \boldsymbol{\theta}', t)$ is the local total density and we define the correlation function $g^{(2)}$ and the cavity correlation function $u^{(2)}$ as

$$\psi^{(2)}(\mathbf{r}, \boldsymbol{\theta}, \mathbf{r}', \boldsymbol{\theta}', t) = \psi^{(1)}(\mathbf{r}, \boldsymbol{\theta}, t) \psi^{(1)}(\mathbf{r}', \boldsymbol{\theta}', t) g^{(2)}(\mathbf{r}, \boldsymbol{\theta}, \mathbf{r}', \boldsymbol{\theta}', t), \quad (2.9a)$$

$$g^{(2)}(\mathbf{r}, \boldsymbol{\theta}, \mathbf{r}', \boldsymbol{\theta}', t) = \exp[-\beta\Phi_{1,2}(\mathbf{r} - \mathbf{r}')] u^{(2)}(\mathbf{r}, \boldsymbol{\theta}, \mathbf{r}', \boldsymbol{\theta}', t). \quad (2.9b)$$

At low densities in equilibrium, $g^{(2)} = \exp[-\beta\Phi_{1,2}(\mathbf{r} - \mathbf{r}')]$, so $u^{(2)} = 1$. So $u^{(2)}$ gives high density corrections and corrections due to the self propulsion. In bulk in equilibrium we have $\int_{B(\mathbf{r}_1, \sigma_{HS})} d\mathbf{r}' \nabla_{\mathbf{r}'-\mathbf{r}} \left(\psi^{(1)}(\mathbf{r}', \boldsymbol{\theta}', t)(u^{(2)}-1) \right) \equiv 0$ due to rotational invariance. In bulk with a low density in equilibrium we have the stronger condition $u^{(2)} \equiv 1$.

2.5 The Closure: The Two-Body Correlation Function

A closure relation is needed for the two-body correlation function $g^{(2)}$. We use the local density approximation and assume the absence of internal torques. Then we derive a PDE for the two-body correlation function $g^{(2)}(\mathbf{r}_{12}, \boldsymbol{\theta}_1, \boldsymbol{\theta}_2)$ in Appendix A.5 from Equation 2.6 and we obtain

$$0 = \frac{\partial g^{(2)}}{\partial t} = - \nabla_{\mathbf{r}_{12}} \cdot \left[\underbrace{\sqrt{3} \text{Pe} (\mathbf{e}(\boldsymbol{\theta}_2) - \mathbf{e}(\boldsymbol{\theta}_1)) g^{(2)}}_{\text{Self propulsion}} + \underbrace{2\mathbf{F}_{12} g^{(2)}}_{\text{Direct interactions}} - \underbrace{2\nabla_{\mathbf{r}_{12}} g^{(2)}}_{\text{Diffusion}} \right. \\ \left. + \underbrace{\iint d\mathbf{r}_3 d\boldsymbol{\theta}_3 (\mathbf{F}_{23} - \mathbf{F}_{13}) \frac{\psi^{(3)}}{(\rho)^2}}_{\text{Three-body correlations}} \right] + \underbrace{\nabla_{\boldsymbol{\theta}_1}^2 g^{(2)} + \nabla_{\boldsymbol{\theta}_2}^2 g^{(2)}}_{\text{Rotational Diffusion}}. \quad (2.10)$$

In the low-density limit the inequality $\psi^{(3)} \ll (\psi^{(1)})^2$ holds and hence the three-body correlations on $\psi^{(3)}$ can be neglected. In 2 dimensions with rotational invariance, the correlation function $g^{(2)}(r, \theta_1 - \phi, \theta_2 - \phi)$ only depends on the absolute distance r and relative orientations $\theta_1 \rightarrow \theta_1 - \phi$ and $\theta_2 \rightarrow \theta_2 - \phi$. Then the PDE for $g^{(2)}(r, \theta_1, \theta_2)$ in relative coordinates becomes closed. It is simplified in Appendix A.6 and given by

$$\frac{\partial g^{(2)}}{\partial t} = - \left[\frac{\partial}{\partial r} \left(\sqrt{3} \text{Pe} (\cos \theta_2 - \cos \theta_1) g^{(2)} + 2F_{12} g^{(2)} - 2\partial_r g^{(2)} \right) \right. \\ \left. + \frac{1}{r} \left(2F_{12} g^{(2)} - 2\partial_r g^{(2)} \right) \right] + \partial_{\theta_1}^2 g^{(2)} + \partial_{\theta_2}^2 g^{(2)} \\ + \left(\frac{\sqrt{3} \text{Pe}}{r} (\sin \theta_2 - \sin \theta_1) \left(\partial_{\theta_1} g^{(2)} + \partial_{\theta_2} g^{(2)} \right) + \frac{2}{r^2} (\partial_{\theta_1} + \partial_{\theta_2})^2 g^{(2)} \right). \quad (2.11)$$

In this low density limit this equation is linear in $g^{(2)}$. In Figure 2.3 an illustration is given of the relative coordinate system. In the next chapter we will derive the asymptotic behavior of Equation 2.11.

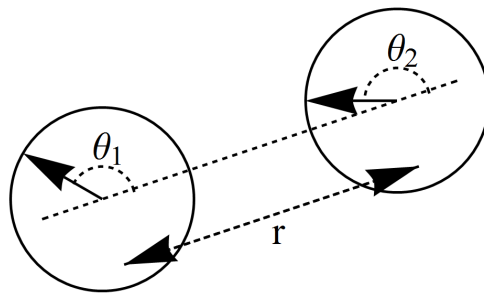


Fig. 2.3 Illustration of the relative coordinate system in 2 dimensions. The arrows within the particles indicate the direction of the self propulsive force.

Chapter 3

Analytic Expression for the Correlation Length

In this chapter we will derive an analytic expression for the correlation length of the two-body correlation function and the one-particle distribution near a wall. The starting point will be Equations 2.7 and 2.11, where we are restricted to the zero density limit in 2 dimensions. Consider only the steady state; the correlation function is constant in time, so $\frac{\partial g^{(2)}}{\partial t} = 0$ and $g^{(2)} = g^{(2)}(r, \theta_1, \theta_2)$. We split the equation into terms scaling with the Peclet number Pe and terms not scaling with Pe . For convenience, multiply the equation by a factor $r^2/2$ to obtain

$$0 = \frac{\sqrt{3} Pe}{2} \left[-(\cos \theta_2 - \cos \theta_1) r^2 \partial_r g^{(2)} + r (\sin \theta_2 - \sin \theta_1) (\partial_{\theta_1} g^{(2)} + \partial_{\theta_2} g^{(2)}) \right] \quad (3.1)$$
$$+ \left(1 + \frac{r^2}{2} \right) (\partial_{\theta_1}^2 g^{(2)} + \partial_{\theta_2}^2 g^{(2)}) - r \partial_r \left(r (F_{12}(r) g^{(2)} - \partial_r g^{(2)}) \right) + 2 \partial_{\theta_1} \partial_{\theta_2} g^{(2)}.$$

3.1 General Expression for the Correlation Function at Distances Larger than the Range of the Force

Next, we consider a Taylor expansion for small Pe and a Fourier expansion in θ_1 and θ_2 at each distance r . In other words, we will substitute

$$g^{(2)}(r, \theta_1, \theta_2) = \sum_{m,n,p \in \mathbb{N}_0} R_{pmn}(r) Pe^p \cos(m\theta_1) \cos(n\theta_2) + S_{pmn}(r) Pe^p \sin(m\theta_1) \sin(n\theta_2) \quad (3.2)$$
$$+ T_{pmn}(r) Pe^p \cos(m\theta_1) \sin(n\theta_2) + U_{pmn}(r) Pe^p \sin(m\theta_1) \cos(n\theta_2)$$

into Equation 3.1, where $\mathbb{N}_0 = \{0, 1, 2, \dots\}$ are the non negative integers including zero, and where $R_{pmn}(r)$, $S_{pmn}(r)$, $T_{pmn}(r)$ and $U_{pmn}(r)$ denote expansion coefficients that are to be determined. The result obtained holds for all $(\text{Pe}, \theta_1, \theta_2)$, so independent components are zero individually. First we define

$$F[X, p, m, n] = \frac{\sqrt{3}r^2}{4} \left[X'_{p-mn_-}(r) + X'_{p-mn_+}(r) - X'_{p-m-n}(r) - X'_{p-m+n}(r) \right. \\ \left. + x^{(2)}X'_{p-,m,1}(r) - x^{(1)}X'_{p-,1,n}(r) \right] \\ - \frac{\sqrt{3}r}{4} \left[n_-X_{p-mn_-}(r) - n_+X_{p-mn_+}(r) - m_-X_{p-m-n}(r) + m_+X_{p-m+n}(r) \right], \quad (3.3)$$

where $X \in \{R, S, T, U\}$ is shorthand notation, $X' = \partial_r X$ is a spatial derivative and the notations $m_{\pm} = m \pm 1$, $n_{\pm} = n \pm 1$ and $p_- = p - 1$ are used for the indices. Further, we defined $x^{(1)} = 1$ if $m = 0$ and $X = R, T$, we defined $x^{(1)} = -1$ if $m = 0$ and $X = S, U$ and we defined $x^{(1)} = 0$ if $m \neq 0$. Similar, we defined $x^{(2)} = 1$ if $m = 0$ and $X = R, U$, we defined $x^{(2)} = -1$ if $m = 0$ and $X = S, T$ and we defined $x^{(2)} = 0$ if $n \neq 0$.

We use Equation 3.3 and substitute Equation 3.2 into Equation 3.1 and conclude

$$F[R, p, m, n] = +2mnS - \left(1 + \frac{1}{2}r^2\right) (m^2 + n^2)R - r\partial_r (r(F_{12}R - \partial_r R)), \quad (3.4a)$$

$$F[S, p, m, n] = +2mnR - \left(1 + \frac{1}{2}r^2\right) (m^2 + n^2)S - r\partial_r (r(F_{12}S - \partial_r S)), \quad (3.4b)$$

$$F[T, p, m, n] = -2mnU - \left(1 + \frac{1}{2}r^2\right) (m^2 + n^2)T - r\partial_r (r(F_{12}T - \partial_r T)), \quad (3.4c)$$

$$F[U, p, m, n] = -2mnT - \left(1 + \frac{1}{2}r^2\right) (m^2 + n^2)U - r\partial_r (r(F_{12}U - \partial_r U)). \quad (3.4d)$$

This holds for all indices p , m and n . These indices are not explicitly denoted in $R = R_{pmn}(r)$, $S = S_{pmn}(r)$, $T = T_{pmn}(r)$ and $U = U_{pmn}(r)$, since the indices within the same equation are all the same. We notice all terms of $F[X, p, m, n]$ are of order $p - 1$ in Pe . For small Peclet numbers, we can therefore treat $F[X, p, m, n]$ as the inhomogeneous part of a partial differential equation. Consider first the low self propulsion speeds, where we obtain the homogeneous equations; i.e. $\text{Pe} \rightarrow 0$ and hence $F[X, p, m, n] \rightarrow 0$. We are left with 4 pairwise coupled partial differential equations, for when $(m, n) \neq (0, 0)$ and the distance¹ is large enough such that $\partial_r \Phi_{12} \equiv 0$. We

¹For a WCA potential [15] at distance $r > 2^{1/6}\sigma = 2^{1/6}\sqrt{3}$.

obtain

$$R_{pmn}(r) = C_{pmn}^+ K_{\alpha_+} \left(\frac{r}{\xi_{mn}} \right) + C_{pmn}^- K_{\alpha_-} \left(\frac{r}{\xi_{mn}} \right), \quad (3.5a)$$

$$S_{pmn}(r) = -C_{pmn}^+ K_{\alpha_+} \left(\frac{r}{\xi_{mn}} \right) + C_{pmn}^- K_{\alpha_-} \left(\frac{r}{\xi_{mn}} \right), \quad (3.5b)$$

$$T_{pmn}(r) = D_{pmn}^+ K_{\alpha_+} \left(\frac{r}{\xi_{mn}} \right) + D_{pmn}^- K_{\alpha_-} \left(\frac{r}{\xi_{mn}} \right), \quad (3.5c)$$

$$U_{pmn}(r) = D_{pmn}^+ K_{\alpha_+} \left(\frac{r}{\xi_{mn}} \right) - D_{pmn}^- K_{\alpha_-} \left(\frac{r}{\xi_{mn}} \right), \quad (3.5d)$$

where $\xi_{mn} = \sqrt{2/(m^2 + n^2)}$ is the correlation length in dimensionless units, it obtains a maximum value for $\xi_0 := \xi_{01} = \xi_{10} = \sqrt{2}$, which equals $\xi_0 = \sqrt{2/3}\sigma$ in terms of the particle diameter σ , and C_{pmn}^\pm and D_{pmn}^\pm are integration constants. Further, K_{α_+} and K_{α_-} are the modified Bessel function which converge asymptotically independent of the coefficient α_\pm to $K_{\alpha_\pm}(x) \rightarrow \sqrt{\pi/2}e^{-x}/\sqrt{x}$. The diverging solutions, also modified Bessel functions $I_{\alpha_\pm}(x)$, are omitted since they are unphysical. The coefficients of the Bessel functions are defined as $\alpha_\pm = \sqrt{m^2 \pm 2mn + n^2} = |m \pm n|$.

Including Low Non-Zero Self Propulsion Speeds

The modes $R_{pmn}(r)$, $S_{pmn}(r)$, $T_{pmn}(r)$ and $U_{pmn}(r)$ with different indices couple if we include non-zero self propulsion speeds. In this section we consider low non-zero self propulsion speeds $0 < \text{Pe} < \text{Pe}_{\text{crit}}$. Numerical results will later show $\text{Pe}_{\text{crit}} \approx 0.1$. Aside from the general solutions (Equation 3.5) obtained from the homogeneous PDE, also particular solutions for the inhomogeneous PDE due to $F[X, p, m, n] \neq 0$ become important. This F introduces a coupling between modes with different correlation lengths in the general solution. As in the homogeneous case, we restrict to distances where the potential vanishes, i.e. $\partial_r \Phi_{12} \equiv 0$. We make the following claim regarding Equation 3.4.

Claim 3.1.1

a) The solutions are all of the following form:

$R, S, T, U = \sum_{\{\xi\}} d_\xi \frac{e^{-r/\xi}}{\sqrt{r}} \times Q_\xi(r)$ with d_ξ constants and Q_ξ functions with the property that $\lim_{r \rightarrow \infty} Q_\xi(r) = 1 + O(1/r)$, i.e. $Q_\xi(r)$ converges to 1.

b) The set of exponents is a subset of the countable set $\{\xi\} \subset \{\sqrt{2}/\sqrt{m^2 + n^2} | m, n \in \mathbb{N}\}$. Furthermore, only exponents, occurring in the homogeneous solution or in the inhomogeneous part $F[X, p, m, n]$, will occur.

We show this by induction.

Proof

Induction basis: All solutions of the homogeneous problem for R, S, T and U are of the form $K_\alpha(r/(\xi_0/\sqrt{m^2 + n^2}))$, see Equation 3.5. It is straightforward to see they satisfy both a) and b). In the lowest order in Pe , the inhomogeneous part becomes trivial; i.e. $F[X, 0, m, n] = 0$. So in the lowest mode of the self propulsion speed ($p = 0$), the claim is satisfied.

Induction Hypothesis: Suppose all modes up to and including order $p - 1$ in Pe are of the form

$$R, S, T, U = \sum_{\{\xi\}} c_\xi \times \frac{e^{-r/\xi}}{\sqrt{r}} \times P_\xi(r) \quad (3.6)$$

with c_ξ constants and P_ξ functions such that $\lim_{r \rightarrow \infty} P_\xi(r) = 1 + O(1/r)$.

Induction Step: Then the inhomogeneous part of the PDE is known, since it only depends on lower order modes and becomes

$$F[X, p, m, n] = \sum_{\{\xi\} \in \Xi_0} \frac{-\sqrt{3}c_\xi r^2}{4/\xi} \times \frac{e^{-r/\xi}}{\sqrt{r}} \times (1 + O(1/r)). \quad (3.7)$$

Further, asymptotically for $r \gg 1$ Equation 3.4 becomes

$$\begin{aligned} F[X, p, m, n] &= \cancel{\pm 2mn\tilde{X}} - \left(\chi + \frac{1}{2}r^2\right) (m^2 + n^2)X - r\partial_r (\cancel{rE_{12}X}) + r^2\partial_r^2 X + \cancel{r\partial_r X} \\ &= r^2 \left[-\frac{1}{2}(m^2 + n^2)X + \partial_r^2 X + O(1/r) \right], \end{aligned} \quad (3.8)$$

since only the terms with an exponential multiplied by r^2 dominate for large values of r . The other terms vanish asymptotically and are stroked out. We have to solve

$$\sum_{\{\xi\} \in \Xi_0} \tilde{c}_\xi \times \frac{e^{-r/\xi}}{\sqrt{r}} \times (1 + O(1/r)) = -\frac{1}{2}(m^2 + n^2)X + \partial_r^2 X + O(1/r), \quad (3.9)$$

which is solved by

$$X = \sum_{\{\xi\} \in \Xi_0 \cup \{\xi_0/\sqrt{m^2+n^2}\}} d_\xi \times \frac{e^{-r/\xi}}{\sqrt{r}} \times \underbrace{[1 + O(1/r)]}_{=: Q_\xi(r)}. \quad (3.10)$$

By induction we have proven the claim of the form of the functions. \square

The Lowest Modes

Now we have another look at the lowest modes of $g(r)$. At $Pe = 0$, the correlation function is isotropic. If $p = m = n = 0$, we obtain the equilibrium result

$$R_{000}(r) = \exp[-\Phi_{12}(r)] \quad (3.11)$$

as we saw before in Equation 1.8b, while all other modes with $p = 0$ are trivial, namely $S_{0mn} = 0$, $T_{0mn} = 0$, $U_{0mn} = 0$ and if $(m, n) \neq (0, 0)$ also $R_{0mn} = 0$. At first order in Pe ($p = 1$), the inhomogeneous part is only nonzero for the $(m, n) = (1, 0), (0, 1)$ mode of R . However, even in these modes the inhomogeneous part vanishes when $\partial_r \Phi_{12} \equiv 0$. Numerically it will turn out that the $(m, n) = (1, 0), (0, 1)$ modes will dominate at low Peclet numbers. These modes are given by the homogeneous solutions we saw before in Equation 3.5a:

$$R_{110}(r) = -R_{101}(r) = C \times K_1(r/\xi_0) \quad (3.12)$$

at distances where $\partial_r \Phi_{12} = 0$ and with C some constant. At higher orders in Pe , the coupling becomes too difficult for an exact analysis beyond the asymptotic limit.

High Self Propulsion Speeds

Our approach breaks down at high self propulsion speeds. Different modes couple to each other with a coupling strength $\sim Pe$. These coupled modes couple again and so on. So the indirect coupling strength is $\sim Pe^n$ from the first modes via $n - 1$ different modes to a final modes. We have thus a power law in n and the indirect coupling strength couples exponentially. For large enough self propulsion speeds $Pe > Pe_{\text{crit}}$, either we need too many terms in the Taylor series in Pe , or the series does not converge at all.

Conclusion About the Correlation Length Between 2 Particles

The longest correlation length is $\xi_0 = \sqrt{2/3}\sigma$ in terms of the particle diameter σ , where the factor $\sqrt{1/3}$ is trivial due to the units chosen. At low Peclet numbers, this correlation length is visible in the modes $\cos\theta_1$ and $\cos\theta_2$, but also in other modes due to the weak coupling between modes. At large Peclet numbers the analytic results are inconclusive.

3.2 One Particle Near a Wall

Let us now start with Equation 2.7 for the one-body distribution function $\psi^{(1)}$ of ideal torque free particles near a planar hard wall. The external force of the hard wall will occur as a no flux boundary condition. We are left with

$$0 = \frac{\partial\psi^{(1)}}{\partial t}(1, t) = -\nabla_{\mathbf{r}} \cdot \left[\sqrt{3}\text{Pe} \mathbf{e}(\boldsymbol{\theta})\psi^{(1)}(1, t) - \nabla_{\mathbf{r}}\psi^{(1)}(1, t) \right] + \nabla_{\boldsymbol{\theta}}^2\psi^{(1)}(1, t). \quad (3.13)$$

We assume that the density profile is translationally invariant perpendicular to the wall; i.e. $\psi^{(1)}(\mathbf{r}, \boldsymbol{\theta}) = \psi^{(1)}(x, \cos\theta)$ where x is the distance to the wall and $\cos\theta$ is the component in direction to the wall of $\mathbf{e}(\boldsymbol{\theta})$. We obtain $\sqrt{3}\text{Pe} \cos\theta \partial_x\psi^{(1)} = \partial_x^2\psi^{(1)} + \partial_{\theta}^2\psi^{(1)}$ in 2D. We make at each distance x a Fourier expansion in θ for the density $\psi^{(1)}(x, \theta) = \sum_{m \geq 0} a_m(x) \cos m\theta$ where the ‘sin’ terms are suppressed because of the symmetry. So Equation 3.13 becomes

$$\begin{aligned} \frac{\sqrt{3}\text{Pe}}{2} \left[\left[\sum_{m \geq 1} \cos m\theta \left[a'_{m-1}(x) + a'_{m+1}(x) \right] \right] + a'_0 \cos\theta + a'_1 \right] \\ = \sum_{m \geq 0} \left[a''_m(x) - m^2 a_m(x) \right] \cos m\theta. \end{aligned} \quad (3.14)$$

If the self propulsion is small enough, the first line can be neglected. Then $a_0(x)$ is a constant and $a_m(x) = c_m \exp[-x/\xi_m]$ for $m > 0$ with correlation length $\xi_m = \sqrt{1/3}\sigma/m$ in terms of the particle diameter σ , where the factor $\sqrt{1/3}$ is trivial due to the chosen units. The longest correlation length is $\xi_1 = \sqrt{1/3}\sigma$, which deviates a factor $\sqrt{2}$ from the longest correlation length ξ_0 between two particles. Including the first line when the self propulsion is large enough, gives a nontrivial coupling between modes.

Chapter 4

Stability Analysis of a Homogeneous Density

In this chapter a stability analysis is made of systems with homogeneous density. We investigate the decay or growth of perturbations in a system. If there exists a homogeneous density and a class of perturbations that grow with time, we have a strong indication of finding phase separation. If all perturbations at some density decay, the system will not spontaneously phase separate. However, we can only conclude a system will not spontaneously phase separate, we cannot conclude a system with a phase separation is unstable.

4.1 Isotropic Correlation Function

We start with Equation 2.8 and restrict ourselves to a bulk system without external forces nor torques, assumed to be homogeneous with a constant one-body distribution $\psi_0^{(1)}$ apart from a small inhomogeneous perturbation $\delta\psi^{(1)}(\mathbf{r}, \boldsymbol{\theta}, t)$. Substituting

$\psi^{(1)}(\mathbf{r}, \boldsymbol{\theta}, t) = \psi_0^{(1)} + \delta\psi^{(1)}(\mathbf{r}, \boldsymbol{\theta}, t)$ into Equation 2.8 gives

$$\begin{aligned}
\frac{\partial \delta\psi^{(1)}}{\partial t}(\mathbf{r}, \boldsymbol{\theta}, t) = & \quad (4.1) \\
& - \nabla_{\mathbf{r}} \cdot \left[\sqrt{3} \text{Pe} \mathbf{e}(\boldsymbol{\theta}) \delta\psi^{(1)}(\mathbf{r}, \boldsymbol{\theta}, t) - \frac{\nabla_{\mathbf{r}} \delta\psi^{(1)}(\mathbf{r}, \boldsymbol{\theta}, t)}{(1 - b\rho_0)^2} \right] + \nabla_{\boldsymbol{\theta}}^2 \delta\psi^{(1)}(\mathbf{r}, \boldsymbol{\theta}, t) \\
& - \psi_0^{(1)} \nabla_{\mathbf{r}} \cdot \iint d\mathbf{r}' d\boldsymbol{\theta}' \left[\mathbf{F}_{12}^{\text{long}} \delta\psi^{(1)}(\mathbf{r}', \boldsymbol{\theta}', t) g^{(2)}(\mathbf{r}, \boldsymbol{\theta}, \mathbf{r}', \boldsymbol{\theta}', t) \right] \\
& - \psi_0^{(1)} \nabla_{\mathbf{r}} \cdot \iint d\mathbf{r}' d\boldsymbol{\theta}' \left[\Gamma_{12} \delta\psi^{(1)}(\mathbf{r}', \boldsymbol{\theta}', t) g^{(2)}(\mathbf{r}, \boldsymbol{\theta}, \mathbf{r}', \boldsymbol{\theta}', t) \right] \quad (\text{Torque free}) \\
& - \psi_0^{(1)} \nabla_{\mathbf{r}} \cdot \left[\delta\psi^{(1)}(\mathbf{r}, \boldsymbol{\theta}, t) \iint d\mathbf{r}' d\boldsymbol{\theta}' \left[\mathbf{F}_{12}^{\text{long}} g^{(2)}(\mathbf{r}, \boldsymbol{\theta}, \mathbf{r}', \boldsymbol{\theta}', t) \right] \right] \quad (\text{Isotropic } g^{(2)}) \\
& - \psi_0^{(1)} \nabla_{\mathbf{r}} \cdot \left[\delta\psi^{(1)}(\mathbf{r}, \boldsymbol{\theta}, t) \iint d\mathbf{r}' d\boldsymbol{\theta}' \left[\Gamma_{12} g^{(2)}(\mathbf{r}, \boldsymbol{\theta}, \mathbf{r}', \boldsymbol{\theta}', t) \right] \right] \quad (\text{Isotropic } g^{(2)}) \\
& - \psi_0^{(1)} \nabla_{\mathbf{r}} \cdot \left[\delta\psi^{(1)}(\mathbf{r}, \boldsymbol{\theta}, t) \int d\boldsymbol{\theta}' \int_{B(\mathbf{r}_1, \sigma_{HS})} d\mathbf{r}' \nabla_{\mathbf{r}' - \mathbf{r}} (u^{(2)} - 1) \right] \quad \text{Isotropic } u^{(2)} \\
& - \psi_0^{(1)} \nabla_{\mathbf{r}} \cdot \int d\boldsymbol{\theta}' \int_{B(\mathbf{r}_1, \sigma_{HS})} d\mathbf{r}' \nabla_{\mathbf{r}' - \mathbf{r}} (\delta\psi^{(1)}(\mathbf{r}', \boldsymbol{\theta}', t) (u^{(2)} - 1)) \quad u^{(2)}(\sigma_{HS}) - 1 \approx 0 \\
& + O(\delta\psi^{(1)})^2,
\end{aligned}$$

where we assume a torque free system, the correlation function is isotropic, i.e. $g^{(2)}(\mathbf{r}, \boldsymbol{\theta}, \mathbf{r}', \boldsymbol{\theta}', t) = g^{(2)}(\mathbf{r} - \mathbf{r}', t)$, and the cavity function $u^{(2)} = e^{+\Phi_{12}^{\text{long}}} g^{(2)}$ approximates $u^{(2)}(\sigma_{HS}) \approx 1$ at a distance σ_{HS} . We only take the terms linear in the perturbation of the density into account. We now consider a Fourier decomposition in both position and orientation; i.e.

$$\delta\psi^{(1)}(\mathbf{k}, \boldsymbol{\omega}, t) = \frac{1}{\sqrt{2\pi}^{\dim \mathbf{r} + \dim \boldsymbol{\theta}}} \iint d\mathbf{r} d\boldsymbol{\theta} \delta\psi^{(1)}(\mathbf{r}, \boldsymbol{\theta}, t) e^{-i\mathbf{r} \cdot \mathbf{k}} e^{-i\boldsymbol{\theta} \cdot \boldsymbol{\omega}}, \quad (4.2a)$$

$$\mathbf{e}(\boldsymbol{\omega}) = \frac{1}{\sqrt{2\pi}^{\dim \boldsymbol{\theta}}} \int d\boldsymbol{\theta} \mathbf{e}(\boldsymbol{\theta}) e^{-i\boldsymbol{\theta} \cdot \boldsymbol{\omega}}, \quad (4.2b)$$

where \mathbf{k} the Fourier transformed variable of \mathbf{r} and $\boldsymbol{\omega}$ the Fourier transformed variable of $\boldsymbol{\theta}$. We obtain

$$\begin{aligned}
\frac{\partial \delta\psi^{(1)}}{\partial t}(\mathbf{k}, \boldsymbol{\omega}, t) = & - i\mathbf{k} \cdot \left[\sqrt{3} \text{Pe} \delta\Psi^{(1)}(\mathbf{k}, \boldsymbol{\omega} + *, t) - \frac{i\mathbf{k} \delta\psi^{(1)}(\mathbf{k}, \boldsymbol{\omega}, t)}{(1 - b\rho_0)^2} \right] \quad (4.3) \\
& - \boldsymbol{\omega}^2 \delta\psi^{(1)}(\mathbf{k}, \boldsymbol{\omega}, t) - i\mathbf{k} \cdot \psi_0^{(1)} \mathbf{F}_{\text{int}}[\delta\psi^{(1)}, \mathbf{k}, \boldsymbol{\omega}, t],
\end{aligned}$$

with the Fourier transformed internal force defined as

$$\mathbf{F}_{\text{int}}[\delta\psi^{(1)}, \mathbf{k}, \boldsymbol{\omega}, t] = \iiint\!\!\!\int d\mathbf{r} d\boldsymbol{\theta} d\mathbf{r}_2 d\boldsymbol{\theta}_2 \quad (4.4)$$

$$\left[\mathbf{F}_{12}^{\text{long}}(\mathbf{r}_2 - \mathbf{r}) g^{(2)}(\mathbf{r}_2 - \mathbf{r}, t) \frac{\delta\psi^{(1)}(\mathbf{r}_2, \boldsymbol{\theta}_2, t) e^{-i\mathbf{r}\cdot\mathbf{k}} e^{-i\boldsymbol{\theta}\cdot\boldsymbol{\omega}}}{2\pi^{\dim \mathbf{r} + \dim \boldsymbol{\theta}}} \right]$$

and the contribution due to the self propulsion, $\delta\Psi^{(1)}(\mathbf{k}, \boldsymbol{\omega} + *, t)$, defined as

$$\delta\Psi^{(1)}(\boldsymbol{\omega} + *) := \frac{1}{2} \begin{pmatrix} \delta\psi^{(1)}(\boldsymbol{\omega} + 1) + \delta\psi^{(1)}(\boldsymbol{\omega} - 1) \\ -i\delta\psi^{(1)}(\boldsymbol{\omega} + 1) + i\delta\psi^{(1)}(\boldsymbol{\omega} - 1) \end{pmatrix} \quad \text{in 2D,} \quad (4.5a)$$

$$\delta\Psi^{(1)}(\boldsymbol{\omega} + *) := \frac{1}{4} \begin{pmatrix} -i\delta\psi^{(1)}\left(\boldsymbol{\omega} + \begin{pmatrix} 1 \\ 1 \end{pmatrix}\right) + i\delta\psi^{(1)}\left(\boldsymbol{\omega} + \begin{pmatrix} -1 \\ -1 \end{pmatrix}\right) + \\ i\delta\psi^{(1)}\left(\boldsymbol{\omega} + \begin{pmatrix} -1 \\ 1 \end{pmatrix}\right) - i\delta\psi^{(1)}\left(\boldsymbol{\omega} + \begin{pmatrix} 1 \\ -1 \end{pmatrix}\right) \\ -\delta\psi^{(1)}\left(\boldsymbol{\omega} + \begin{pmatrix} 1 \\ 1 \end{pmatrix}\right) - \delta\psi^{(1)}\left(\boldsymbol{\omega} + \begin{pmatrix} -1 \\ -1 \end{pmatrix}\right) + \\ \delta\psi^{(1)}\left(\boldsymbol{\omega} + \begin{pmatrix} -1 \\ 1 \end{pmatrix}\right) + \delta\psi^{(1)}\left(\boldsymbol{\omega} + \begin{pmatrix} 1 \\ -1 \end{pmatrix}\right) + \\ 2\delta\psi^{(1)}\left(\boldsymbol{\omega} + \begin{pmatrix} 1 \\ 0 \end{pmatrix}\right) + 2\delta\psi^{(1)}\left(\boldsymbol{\omega} + \begin{pmatrix} -1 \\ 0 \end{pmatrix}\right) \end{pmatrix} \quad \text{in 3D,} \quad (4.5b)$$

where we suppress the arguments \mathbf{k} and t . In the three dimensional case we use the convention

$$\mathbf{e}(\boldsymbol{\theta}) = (\cos \boldsymbol{\theta}^{(2)} \sin \boldsymbol{\theta}^{(1)}, \sin \boldsymbol{\theta}^{(2)} \sin \boldsymbol{\theta}^{(1)}, \cos \boldsymbol{\theta}^{(1)}). \quad (4.6)$$

4.2 Unstable or Stable Perturbations to a Homogeneous Density

Define the M dimensional vector $\delta\boldsymbol{\psi}_t$ for all times t , where each component is given by a mode $\delta\psi^{(1)}(\mathbf{k}, \boldsymbol{\omega}, t)$ and different components have different $(\mathbf{k}, \boldsymbol{\omega})$. We notice the set of all modes is countable under assumption of a finite (possibly large) volume. We only include the M lowest (dominant) modes in the orientation space and we require that if mode $\boldsymbol{\omega}$ is included, also mode $-\boldsymbol{\omega}$ be included, where M can be arbitrarily large. We assume only a finite number of modes gives a significant contribution and we can neglect the other modes. The problem of Equation 4.3 is reduced to a linear algebra problem. For every t we have

$$\partial_t \delta\boldsymbol{\psi}_t = (D^t + iA^t) \delta\boldsymbol{\psi}_t \quad (4.7)$$

where D^t and A^t are $M \times M$ matrices. It will be straightforward to see that these matrices are Hermitian, when these matrices are explicitly denoted. For any vector $\delta\psi_t$, we have

$$\frac{\delta\psi_t^* (D^t + iA^t) \delta\psi_t}{\delta\psi_t^* \delta\psi_t} = \underbrace{\frac{\delta\psi_t^* D^t \delta\psi_t}{\delta\psi_t^* \delta\psi_t}}_{\in [\min \sigma_{D^t}, \max \sigma_{D^t}]} + i \underbrace{\left[\frac{\delta\psi_t^* A^t \delta\psi_t}{\delta\psi_t^* \delta\psi_t} \right]}_{\in \mathbb{R}}, \quad (4.8)$$

where the $*$ denote the conjugated transposed. The domains of the terms on the right hand side (also called Rayleigh Quotients), are straightforward when we consider that all eigenvalue of Hermitian matrices are real valued and all vectors can be decomposed in terms of the eigenvectors. Thus conclude for any eigenvalue λ of the matrix $D^k + iA^t$ with eigenvector $\delta\psi_t$ that

$$\begin{aligned} \Re\lambda &= \Re \frac{\delta\psi_t^* \lambda \delta\psi_t}{\delta\psi_t^* \delta\psi_t} = \Re \frac{\delta\psi_t^* (D^t + iA^t) \delta\psi_t}{\delta\psi_t^* \delta\psi_t} \\ &= \Re \frac{\delta\psi_t^* D^t \delta\psi_t}{\delta\psi_t^* \delta\psi_t} \leq \underbrace{\max \sigma_{D^t}}_{\max \text{ eigenvalue}}. \end{aligned} \quad (4.9)$$

Thus if the maximum eigenvalue of D^t is negative, the real part of any eigenvalue of $D^k + iA^t$ is negative. We stress we have not found any eigenvalues of $D^t + iA^t$ explicitly, since the eigenvectors may differ from the eigenvectors of D^t . Fortunately, we are only interested in the sign of the real part. If this real part is negative for all densities ρ_0 , all modes $\mathbf{k} \neq \mathbf{0}$ and all modes ω , then we can conclude that this homogeneous systems is stable. Therefore, these systems will not spontaneously phase separate. We can exclude the $\mathbf{k} = \mathbf{0}$ mode since it violates particle number conservation. Although these systems do not spontaneously phase separate, we have not excluded the possibility that a phase separated system is also stable and possibly energetically favorable.

4.3 MIPS with Isotropic Correlation Function

Suppose the particles only have an excluded volume contribution; i.e. they do not have any attractions (or long ranged repulsions) thus $\mathbf{F}_{12}^{\text{long}} = 0$ and $\mathbf{F}_{\text{int}} = 0$ in Equation 4.3.

Our system to solve is then given by

$$\partial_t \delta\psi_{\mathbf{k}} = \left(D^{\mathbf{k}} + iA^{\mathbf{k}} \right) \delta\psi_{\mathbf{k}}, \quad (4.10a)$$

$$D_{ij}^{\mathbf{k}} = \begin{cases} -\frac{\mathbf{k}^2}{(1-b\rho_0)^2} - \omega_i^2 & \omega_i = \omega_j \\ 0 & \text{otherwise} \end{cases}, \quad (4.10b)$$

$$A_{ij}^{\mathbf{k}} = \begin{cases} -\frac{\sqrt{3}Pe}{2} \mathbf{k} \cdot \begin{pmatrix} 1 \\ \mp i \end{pmatrix} & \omega_i - \omega_j = \pm 1 \text{ in 2D} \\ -\frac{\sqrt{3}Pe}{4} \mathbf{k} \cdot \begin{pmatrix} \mp i \\ 1 \\ 0 \end{pmatrix} & \omega_i - \omega_j = \begin{pmatrix} \pm 1 \\ \mp 1 \end{pmatrix} \text{ in 3D} \\ -\frac{\sqrt{3}Pe}{4} \mathbf{k} \cdot \begin{pmatrix} \mp i \\ -1 \\ 0 \end{pmatrix} & \omega_i - \omega_j = \begin{pmatrix} \pm 1 \\ \pm 1 \end{pmatrix} \text{ in 3D} \\ -\frac{\sqrt{3}Pe}{2} \mathbf{k} \cdot \begin{pmatrix} 0 \\ 0 \\ 1 \end{pmatrix} & \omega_i - \omega_j = \begin{pmatrix} \pm 1 \\ 0 \end{pmatrix} \text{ in 3D} \\ 0 & \text{otherwise (both 2D and 3D)}. \end{cases} \quad (4.10c)$$

It is straightforward to see both $D^{\mathbf{k}}$ and $A^{\mathbf{k}}$ are Hermitian, and that for $\mathbf{k} \neq \mathbf{0}$ all eigenvalues of $D^{\mathbf{k}}$ are negative. A perturbation with $\mathbf{k} = \mathbf{0}$ would violate total density conservation and is not allowed. From the analysis in Section 4.2 we conclude that all eigenvalues of $D^{\mathbf{k}} + iA^{\mathbf{k}}$ are negative and that the system will not spontaneously form MIPS.

4.4 Considering the Force in the Stability Analysis

Let us have another look at the Fourier transform of the internal force, see Equation 4.4. This internal force is a Fourier transform of a convolution, which is the product of the Fourier transformed functions:

$$\mathbf{F}_{\text{int}}[\delta\psi^{(1)}, \mathbf{k}, \omega, t] = \mathcal{F} \left[\mathbf{F}_{12} g^{(2)} \right] \cdot \underbrace{\mathcal{F} \left[\delta\psi^{(1)} \right]}_{\delta\psi^{(1)}(\mathbf{k}, \omega, t)}. \quad (4.11)$$

The Fourier transform of the force is given by

$$-i\mathbf{k} \cdot \mathcal{F} \left[\mathbf{F}_{12} g^{(2)} \right] = i\mathbf{k} \cdot \mathcal{F} \left[\nabla_{\mathbf{r}} \Phi_{12}^{\text{eff}} \right] = -\mathbf{k}^2 \mathcal{F} \left[\Phi_{12}^{\text{eff}} \right], \quad (4.12)$$

where we defined $\nabla_{\mathbf{r}} \Phi_{12}^{\text{eff}}(\mathbf{r}) := -\mathbf{F}_{12}^{\text{eff}}(\mathbf{r}) := -\mathbf{F}_{12}(\mathbf{r})g^{(2)}(\mathbf{r})$. For physical liquids and gases, the effective potential is smooth, bounded and has a well defined Fourier transform. Assume the effective potential is zero if the distance is large enough (or introduce a cutoff). Define the distance r_c as the minimal distance such that $\forall |\mathbf{r}| > r_c$,

$\Phi_{12}^{\text{eff}}(\mathbf{r}) = 0$. For a small wavenumber \mathbf{k} with $|\mathbf{k}|r_c \leq \pi/2$, we can determine the sign of $\mathcal{F}[\Phi_{12}^{\text{eff}}](\mathbf{k})$ if Φ_{12} is purely repulsive or purely attractive and we conclude

$$\begin{cases} -i\mathbf{k} \cdot \mathcal{F}[\mathbf{F}_{12}g^{(2)}](\mathbf{k}) \geq 0 & \text{if } \forall \mathbf{r}_{12} \text{ s.t. } \mathbf{F}_{12} \cdot \mathbf{r}_{12} \leq 0 \text{ (only attractions),} \\ -i\mathbf{k} \cdot \mathcal{F}[\mathbf{F}_{12}g^{(2)}](\mathbf{k}) \leq 0 & \text{if } \forall \mathbf{r}_{12} \text{ s.t. } \mathbf{F}_{12} \cdot \mathbf{r}_{12} \geq 0 \text{ (only repulsions).} \end{cases} \quad (4.13)$$

The validation of this statement is straightforward for $|\mathbf{k}|r_c \leq \pi/2$; it follows from the definition of the Fourier transform. When $\pi/2 < |\mathbf{k}|r_c \leq \pi$ we have to use the definition of the Fourier transform and the property $|\Phi_{12}^{\text{eff}}(\mathbf{r})| > |\Phi_{12}^{\text{eff}}(\mathbf{r}')|$ if and only if $|\mathbf{r}| < |\mathbf{r}'|$. For $|\mathbf{k}| > \pi$ the statement does not hold and a counterexample can be constructed when $\mathbf{F}_{12}(\mathbf{r})g^{(2)}(\mathbf{r})$ is only significantly different from zero for $|\mathbf{r}|$ near r_c . A corresponding physical system consist of particles that approximately¹ have hard cores; thus for $r < r_c - \epsilon$ the correlation function is zero for small $\epsilon > 0$.

We emphasize that when we do not make the excluded volume approximation, we can extend this conclusion also to the short ranged forces. A concern might be that the potential diverges at zero distance and the Fourier transform is ill defined. However, the effective potential will be bounded due to the correlation function.

4.5 The Stability Analysis Without the Excluded Volume Approximation

One could argue that our result in Section 4.3 that spontaneous phase separations will not occur, is caused by the excluded volume treatment of the short ranged forces. However, this excluded volume treatment is not the problem, as we will argue now. Suppose we would not have made the excluded volume treatment in a model without attraction, then Equation 4.3 becomes

$$\begin{aligned} \frac{\partial \delta\psi^{(1)}}{\partial t}(\mathbf{k}, \boldsymbol{\omega}, t) = & -i\mathbf{k} \cdot \left[\sqrt{3} \text{Pe} \delta\Psi^{(1)}(\mathbf{k}, \boldsymbol{\omega} + *, t) - i\mathbf{k} \delta\psi^{(1)}(\mathbf{k}, \boldsymbol{\omega}, t) \right] \\ & - \boldsymbol{\omega}^2 \delta\psi^{(1)}(\mathbf{k}, \boldsymbol{\omega}, t) - i\mathbf{k} \cdot \psi_0^{(1)} \mathbf{F}_{\text{int}}[\delta\psi^{(1)}, \mathbf{k}, \boldsymbol{\omega}, t], \end{aligned} \quad (4.14)$$

¹Approximately such that the force is well defined.

where now F_{int} contributes for the (short-ranged) repulsions, i.e.

$$\mathbf{F}_{\text{int}}[\delta\psi^{(1)}, \mathbf{k}, \boldsymbol{\omega}, t] = \iiint\!\!\!\int d\mathbf{r} d\boldsymbol{\theta} d\mathbf{r}_2 d\boldsymbol{\theta}_2 \quad (4.15)$$

$$\left[\mathbf{F}_{12}^{\text{rep}}(\mathbf{r}_2 - \mathbf{r}) g^{(2)}(\mathbf{r}_2 - \mathbf{r}, t) \frac{\delta\psi^{(1)}(\mathbf{r}_2, \boldsymbol{\theta}_2, t) e^{-i\mathbf{r}\cdot\mathbf{k}} e^{-i\boldsymbol{\theta}\cdot\boldsymbol{\omega}}}{2\pi^{\dim r + \dim \boldsymbol{\theta}}} \right].$$

We find a coupling between different $\boldsymbol{\omega}$ and between different \mathbf{k} modes. Let ψ_t be a vector of the lowest modes in both position and orientation space. We find

$$\partial_t \delta\psi_t = (D^t + iA^t) \delta\psi_t, \quad (4.16a)$$

$$D_{ij}^t = \begin{cases} -\mathbf{k}^2 - \omega_i^2 - i\mathbf{k} \cdot \psi_0^{(1)} \mathcal{F} [\mathbf{F}_{12}^{\text{rep}} g^{(2)}] & \omega_i = \omega_j \\ 0 & \text{otherwise} \end{cases}, \quad (4.16b)$$

where A_{ij}^t is similar to Equation 4.10c. For small values of $|\mathbf{k}|r_c < \pi$ we use Equation 4.13 to conclude $-i\mathbf{k} \cdot \psi_0^{(1)} \mathcal{F} [\mathbf{F}_{12}^{\text{rep}} g^{(2)}] < 0$. We use the result from Section 4.2 to conclude that the matrix $D^t + iA^t$ does not have an eigenvalue with a positive real part for small values of $|\mathbf{k}|$. For large values of $|\mathbf{k}|$, the fluctuations will be on the length scale of a particle; here it is also not possible to find (large) domains of MIPS. We conclude again that the system will not spontaneously phase separate to MIPS. We conclude that this lack of spontaneous MIPS is not an artifact of the excluded volume approximation, but is an artifact of the assumption that the correlation function is isotropic.

4.6 Stability Analysis of a Van der Waals Gas in Equilibrium

In Van der Waals theory in equilibrium, we could also do the same analysis as in Section 4.2. We start with

$$\partial_t \delta\psi_t = (D^t + iA^t) \delta\psi_t, \quad (4.17a)$$

$$D_{ij}^t = \begin{cases} -\frac{\mathbf{k}^2}{(1-b\rho_0)^2} - \omega_i^2 - i\mathbf{k} \cdot \psi_0^{(1)} \mathcal{F} [\mathbf{F}_{12}^{\text{att}}] & \omega_i = \omega_j \\ 0 & \text{otherwise} \end{cases}, \quad (4.17b)$$

$$A_{ij}^t = 0, \quad (4.17c)$$

where $\mathbf{F}_{12}^{\text{att}}$ are the attractions, and there are no correlations, $g^{(2)} = 1$. Assume the largest eigenvalue of D^t is given by a smallest nonzero $|\mathbf{k}|$ and $\omega_i^2 = 0$. This assumption has an intuitive reasoning; the phase separated system with the lowest free energy has two large domains (thus a small $|\mathbf{k}|$ mode is dominant) and is isotropic (zero ω_i). At the (local) spinodal densities in a phase separated system, the densities are barely stable and the largest eigenvalue will be zero. To find the densities, we have to solve

$$0 = \max \sigma_{D^t} = -\omega_i^2 - \mathbf{k}^2 \left[\frac{1}{(1-b\rho)^2} + \psi^{(1)} \mathcal{F} [\Phi_{12}^{\text{att}}] (\mathbf{k}) \right] \quad (4.18)$$

for $\mathbf{0} \neq \mathbf{k} \rightarrow \mathbf{0}$ and $\omega = 0$ and we use $\psi^{(1)} \mathcal{F} [\Phi_{12}^{\text{att}}] (\mathbf{k} \rightarrow 0) = \rho \int d\mathbf{r} \Phi_{12}^{\text{att}}(\mathbf{r}) = -2a\rho/k_B T$ to simplify to $0 = \frac{1}{(1-b\rho)^2} - \frac{2a\rho}{k_B T_c}$. At the critical temperature, the two densities should coincide and be maximal, thus $0 = \partial_{\rho_c} b\rho_c(1-b\rho_c)^2$. This equation is solved by the critical density $\rho_c = 1/3b$ and temperature $k_B T_c = 8a/27b$ and agrees with Equation 1.4.

4.7 Stability Analysis of a Van der Waals Theory out of Equilibrium

If we do the same analysis as in the previous Section 4.6 and include a (small) self propulsion speed, our matrix A^t is no longer zero. Although the upper bound of the real part of the eigenvalues does not change, the real part of the eigenvalues could be smaller; the eigenvalues of D^t and $D^t + iA^t$ are not necessarily equal.

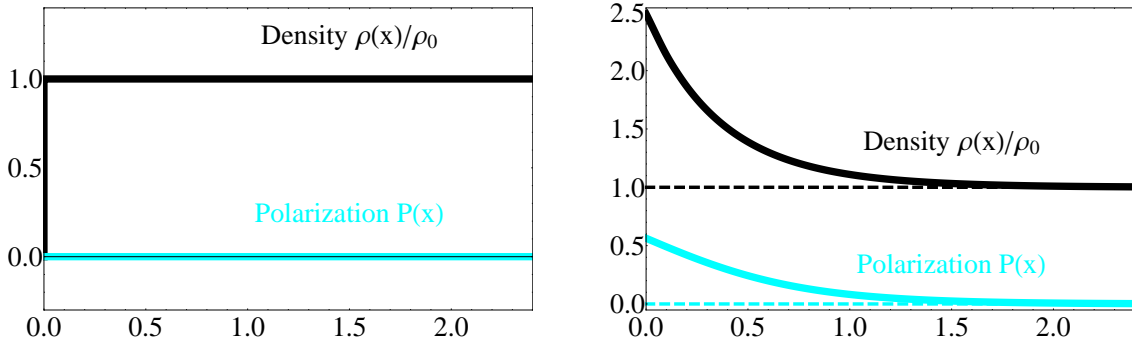
Suppose there exists an eigenvalue of D^t with positive real part. The analysis is inconclusive; we cannot exclude phase separation. Then it is possible that the real part of all the eigenvalues of $D^t + iA^t$ are negative. Thus all perturbations decay, the homogeneous density is stable and phase separation will not occur spontaneously. To find the spinodals and the critical temperature out of equilibrium, we need the maximum real part of the eigenvalues of $D^t + iA^t$; an upper bound is no longer sufficient if it does not give the maximum real part of the eigenvalue. Calculating these eigenvalues is beyond the scope of this thesis.

Chapter 5

Numerical Results

5.1 The Correlation Length of Ideal Particles Near a Wall

In this section we describe the behavior of an active ideal 2 dimensional gas near a hard wall on basis of Equation 2.8. In Figure 5.1 the density profile, as defined in Equation 1.5, and polarization, as defined in Equation 1.6, are plotted. In equilibrium, the profiles of an ideal gas near a hard wall are trivial, see Figure 5.1a. When the self propulsive speed is taken into account, non trivial results are found in Figure 5.1b. Near the wall, particles pile up and have a non zero polarization. Our results are similar to [13].



(a) In equilibrium, $Pe = 0$, the density and the polarization profiles of an ideal gas are trivial.

(b) The solid lines are for $Pe = 1$, a nontrivial profile near the wall is found. The dashed lines are the equilibrium results.

Fig. 5.1 Shown are the density and polarization profile in equilibrium ($Pe = 0$) and for an active fluid ($Pe = 1$).

To explain our non trivial results, we first examine the orientation-dependent distribution $\psi^{(1)}$. In Figure 5.2 the distribution is shown for fixed orientations as a function of distance from the wall. Particles with an orientation towards the wall (blue) will swim towards the wall and pile up against the wall; an increased probability is found. Particles with an orientation away from the wall (red) will instantly swim away, thus a decreased probability is found. For particles with no relative motion with respect to the wall (green) have a slight increased probability of being found near the wall, possibly due to the rotational diffusion of the particles that have a high probability of pointing towards the wall.

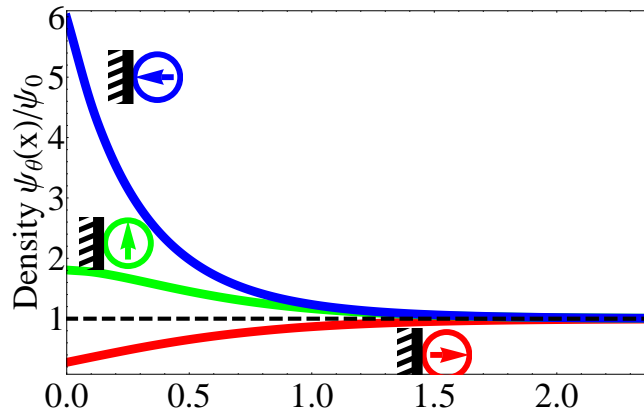


Fig. 5.2 The density profile for an active 2-dimensional ideal particles near a hard wall is shown with Peclet number $Pe = 1$. Different lines represent different orientations.

In Figure 5.3 the asymptotic decay of the density profiles and the polarization profiles are plotted. Different colors represent different Peclet numbers, see the caption. The dashed lines are fits of an exponential $A \exp[-x/\xi]$ with ξ the correlation length and A the amplitude.

In Figure 5.4 the fitting parameters are shown. In Figure 5.4a we observe that the correlation lengths obtained from polarization profiles (red +) and the correlations lengths obtained from the density profiles (blue \times) stay close. The data from the polarization profiles are slightly more accurate, since the amplitudes here are also larger. The analytic correlation length at low self propulsion speeds $\xi = \sqrt{1/3}\sigma$ is found for low Peclet numbers in terms of the particle diameter $\sigma = \sqrt{3}\sqrt{D_t/D_r}$. For high Peclet numbers we find deviations.

In Figure 5.4b the amplitudes are shown as a function of Peclet number. For small Peclet numbers this amplitude scales linearly for the polarizations and quadratically for the densities. This scaling does not hold for large Peclet numbers; here we probably see an artifact of the deviation in the correlation length.

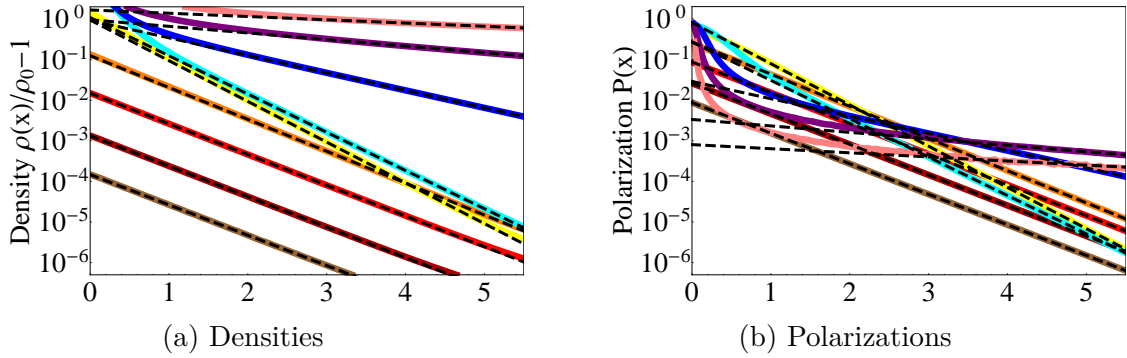
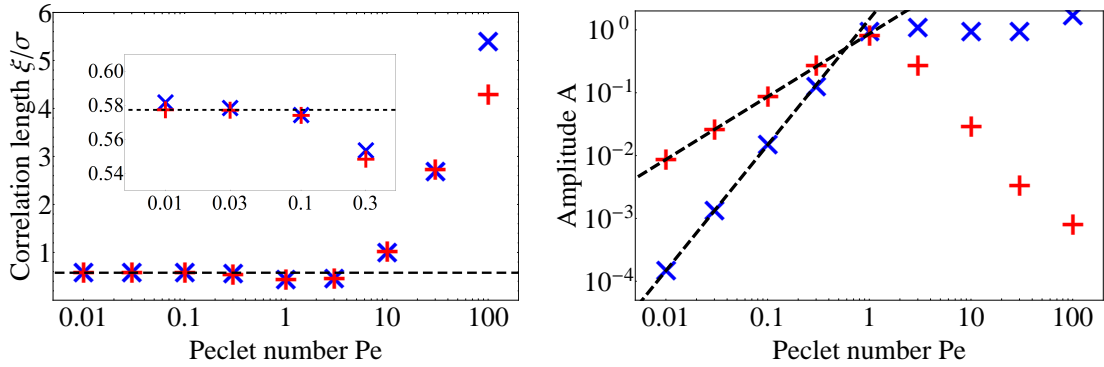


Fig. 5.3 Shown is the decay of the densities and polarizations of an ideal 2-dimensional active gas near a hard wall for different Peclet numbers. The Peclet numbers 0.01 (brown), 0.03 (dark red), 0.1 (red), 0.3 (orange), 1 (yellow), 3 (cyan), 10 (blue), 30 (purple) and 100 (pink) are shown. The dashed black lines are fits of an exponential $A \exp[-x/\xi]$ with ξ the correlation length and A the amplitude.



(a) The correlation lengths in terms of the particle diameter σ are shown for the densities (blue \times) and these agree with the correlation lengths obtained from the polarizations (red $+$). The dashed line is the analytic value for small Peclet numbers $\xi = \sqrt{1/3}\sigma$ in terms of the particle diameter σ . The factor $\sqrt{1/3}$ is trivial due to the choice of units. In the inset a zoom is shown.

(b) The amplitudes of the density (blue \times) and polarization (red $+$) profiles are shown. For small Peclet numbers, the amplitude scales linear for the polarization and quadratic for the densities. These scalings are illustrated by the dashed line. The amplitude of the polarizations appears to scale with $\sim \text{Pe}^{-2}$ and the amplitude of the densities appears to be constant for large Peclet numbers. However, we have not found an analytic expression.

Fig. 5.4 The correlation lengths and amplitudes obtained from the fit of particles near a wall is illustrated as a function of Peclet number. These are shown for the densities (blue crosses \times) and for the polarizations (red plus $+$).

5.2 The Pair Correlation Function $g_{\rho=0}^{(2)}$ in 2D

In this section the results of the pair correlation function $g^{(2)}$ are described. We were only able to calculate this function in the zero density limit in 2 dimensions.

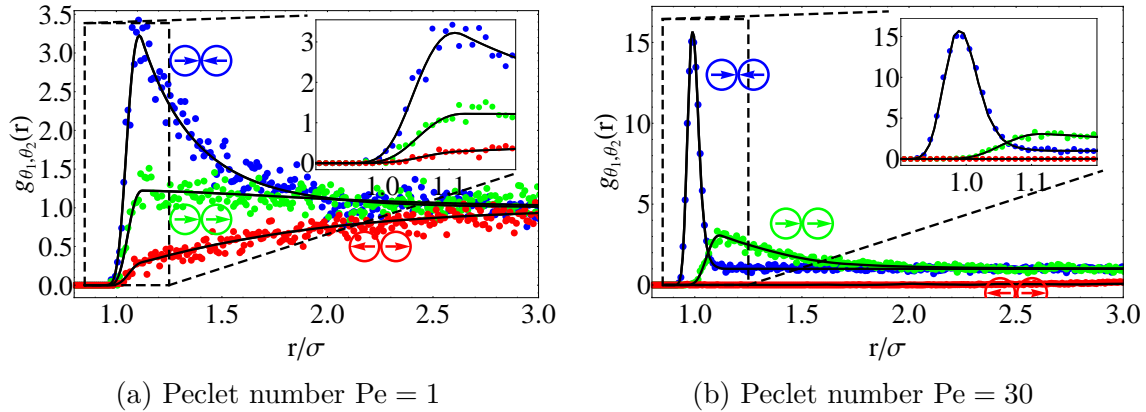


Fig. 5.5 The two-body correlation function $g_{\theta_1, \theta_2}^{(2)}(r)$ as a function of distance for fixed orientations. A WCA potential with $\beta\epsilon = 3$ is used. The lines are obtained from the Fokker-Planck equation, the points are obtained from simulating the EOMs of 1020 particles at a density $\rho\sigma^2 = 0.01$. The simulations were done by Siddharth Paliwal. In blue the particles point towards each other, in green the particles are parallel and in red the particles point away from each other. In the inset a zoomed image is shown.

In Figure 5.5 the pair correlation function $g_{\theta_1, \theta_2}^{(2)}$ is shown for three orientations of two particles. The particles have a Weeks-Chandler-Anderson (WCA) potential¹ [15] and a dimensionless self propulsion $Pe = 1, 30$. At small distances, a pair of particles that point to each other (blue) have an increased probability to be found, while a pair of particles that point away from each other (red) have a reduced probability to be found. The increased probability of particles pointing towards each other can be explained as follows: the particles swim to each other and ‘stick’ together, which increases the probability compared to long distances. They cannot pass through each other. Rotational diffusion makes the particles turn. When the particles point in opposite directions, they instantly swim away; the probability of finding a pair of particles that has not swum away is low.

The results obtained from the F-P equation (full lines) agree with results from simulations of many individual particles [8] (points) where the EOM’s are evaluated for all particles at a low density of $\sigma^2\rho = 0.01$. We stress that the results match without

¹A WCA potential is purely repulsive; it’s the repulsive part of a Lennard-Jones potential.

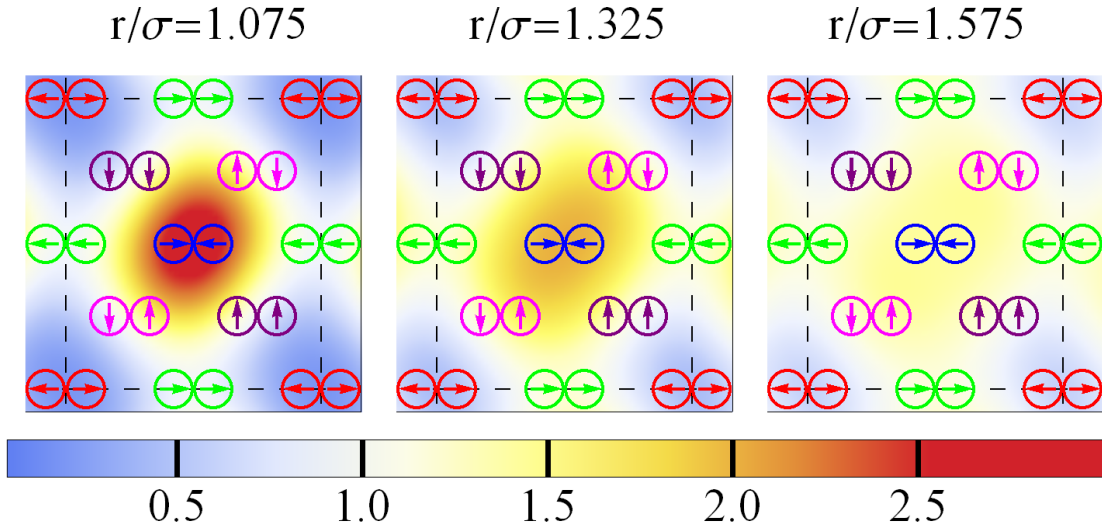


Fig. 5.6 The two-body correlation function $g_r^{(2)}(\theta_1, \theta_2)$ is shown as a function of the orientations for fixed distances. Again a WCA potential with $\beta\epsilon = 3$ and Peclet number $Pe = 1$ is used. It is likely to find particles close together that are pointing towards each other. The dashed lines represent the periodic boundaries of the orientations.

any fitting procedure. Notice that the reduction of noise in simulations requires a larger number of measurements to average and thus a larger computational time, while the F-P equation is less sensitive to noise². The computation of the correlation function using simulations is similar at nonzero densities. In contrast, the computation of the correlation function using the F-P equation becomes very hard; three particle correlations have to be included or even another approach like Ornstein-Zernike is required [14, Ch. 6.2.5].

We show the orientation dependence of the two-body correlation function $g_r^{(2)}(\theta_1, \theta_2)$ at different fixed distances in Figure 5.6. In agreement with the previous Figure 5.5 we conclude particles close to each other are likely to point to each other and unlikely to point away from each other.

5.3 The Correlation Length of the Correlation Function

In Chapter 3 we found an analytic expression for the asymptotic behavior of the correlation function. Now we fit the analytic expression to the result of the F-P

²As long as the derivatives of the distribution functions are not too big. Otherwise additional mesh refinement are needed which increases computing time and memory usages dramatically.

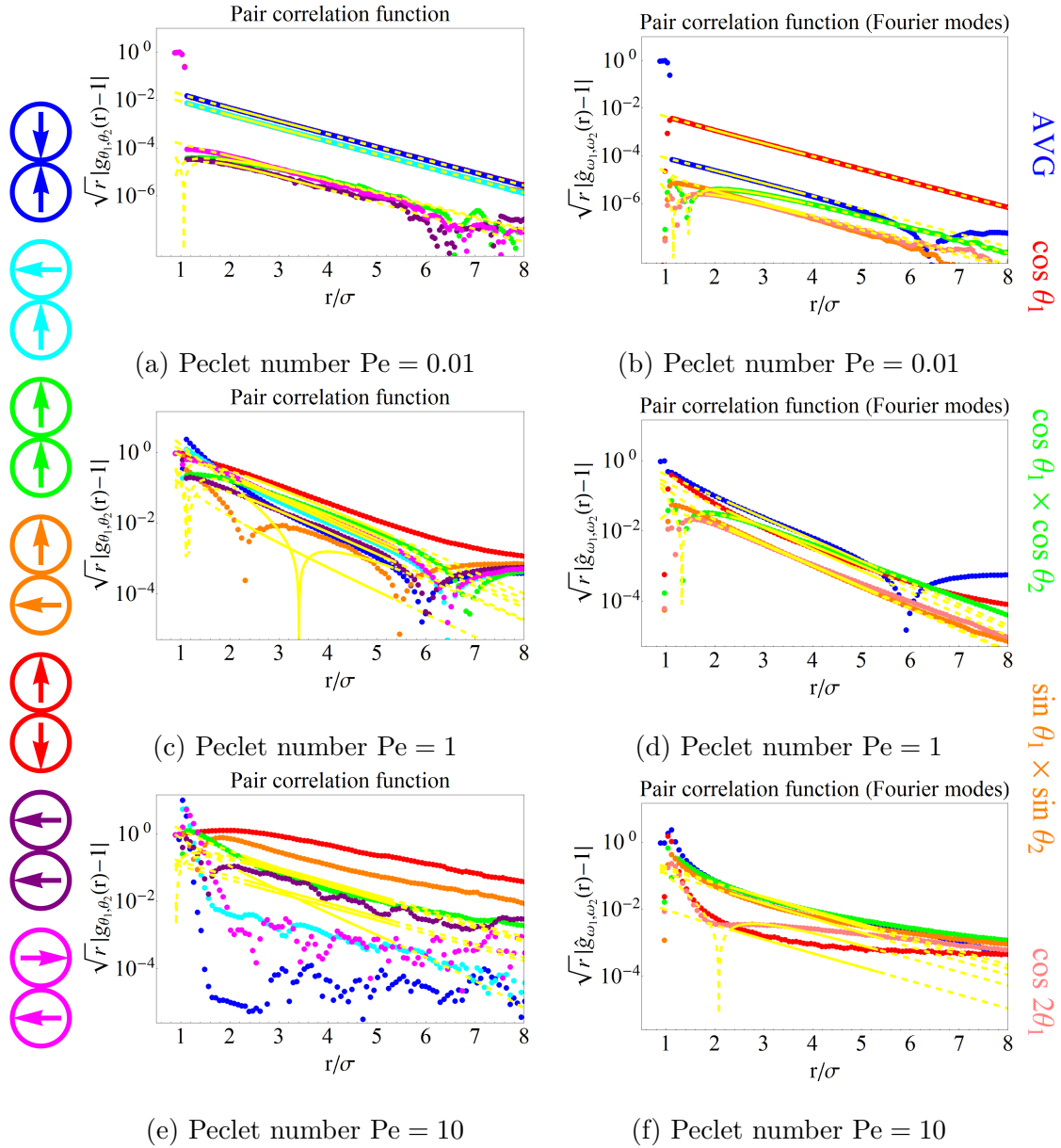


Fig. 5.7 The pair correlation function is shown for different orientations and different Fourier modes, as a function of distance r for different Peclet numbers Pe . All figures represent the zero density limit for particles in a WCA potential with $\beta\epsilon = 3$. The points are the result of numerical evaluation of the F-P equation. Different colors represent different orientations (on the left in Figure a, c or e) or different Fourier modes (on the right in Figure b, d or f). The solid yellow lines are a fit of the data in that range, and the dashed yellow lines are extrapolations.

equation. We include only the lowest modes of the analytic expression, otherwise the number of fitting parameters will be too large. The model used is only suitable for distances where the particles do not apply a force to each other, i.e. $\partial_r \Phi_{12} \equiv 0$. We fit the shape

$$\begin{aligned}
g_{\partial_r \Phi_{12} \equiv 0}^{(2)}(\theta_1, \theta_2, r) = & 1 + \left(C_{110}^+ + C_{110}^- \right) K_1[r/\xi_0] [\cos \theta_2 - \cos \theta_1] \\
& + \left(C_{220}^+ + C_{220}^- \right) K_2[2r/\xi_0] [\cos 2\theta_2 + \cos 2\theta_1] \\
& + \left(C_{220}^+ - C_{220}^- \right) K_2[2r/\xi_0] [\sin 2\theta_2 + \sin 2\theta_1] \\
& + \left(C_{211}^+ K_2[\sqrt{2}r/\xi_0] + C_{211}^- K_0[\sqrt{2}r/\xi_0] \right) \cos \theta_1 \cos \theta_2 \\
& + \left(C_{211}^+ K_2[\sqrt{2}r/\xi_0] - C_{211}^- K_0[\sqrt{2}r/\xi_0] \right) \sin \theta_1 \sin \theta_2 \\
& + \frac{\exp[-r/\xi_0]}{\sqrt{r}} \left\{ E_0 + E_1 \cos \theta_1 \cos \theta_2 + E_2 \sin \theta_1 \sin \theta_2 + \right. \\
& \left. + E_3(\cos 2\theta_2 + \cos 2\theta_1) + E_4(\sin 2\theta_2 + \sin 2\theta_1) \right\}
\end{aligned} \tag{5.1}$$

to the pair correlation function, where the terms scaling with $\frac{\exp[-r/\xi_0]}{\sqrt{r}}$ (last two lines) are only asymptotically correct; we do not know the exact shape due to the coupling between the R_{100} mode and other modes. We used some symmetries already; mirror symmetry implies $C_{pmn}^+ = C_{pmn}^-$ for $m+n$ odd and the exchange of particles implies $C_{pmn}^\pm = (-1)^{m+n} C_{pnm}^\pm$ for any m, n . We will fit the parameters C_{pmn}^\pm , E_i and ξ_0 .

In Figure 5.7 the asymptotic behavior of $|g_{\text{Pe}, \theta_1, \theta_2}(r) - 1|$ is shown for different orientations and different Fourier modes. For a low self propulsion speed, i.e. $\text{Pe} = 0.01$ in Figures 5.7a and 5.7b, our fits of the analytic shape match the data. For medium or high self propulsion speeds, i.e. $\text{Pe} = 1$ in Figures 5.7c and 5.7d or $\text{Pe} = 10$ in Figures 5.7e and 5.7f, the fits deviate from the data.

The deviation between the data from the F-P equation and the fit at large self propulsion speed can have different causes; this deviation can be caused by the data or the used fit function. Firstly, there appear to be some systematic errors in the data, i.e. in Figure 5.7c several lines pass through 0 when $r/\sigma \approx 7$. This passing through 0 has no physical explanation at $r/\sigma \approx 7$. The noise in the data for higher self propulsion is larger, so we cannot exclude this passing through 0. Secondly, the analytic model consist of multiple Fourier modes and modes in self-propulsion speeds, where we only included the lowest modes, see Equation 5.1. At low self propulsion speeds, only the lowest modes contribute and the modes are decoupled, so the analytic result is accurate. At larger self propulsion speed, the analytic model is not accurate.

In Figure 5.8 the maximum correlation length ξ_0 is shown. We show both the analytic result as the result obtained from the fit. Again, for the low self propulsion

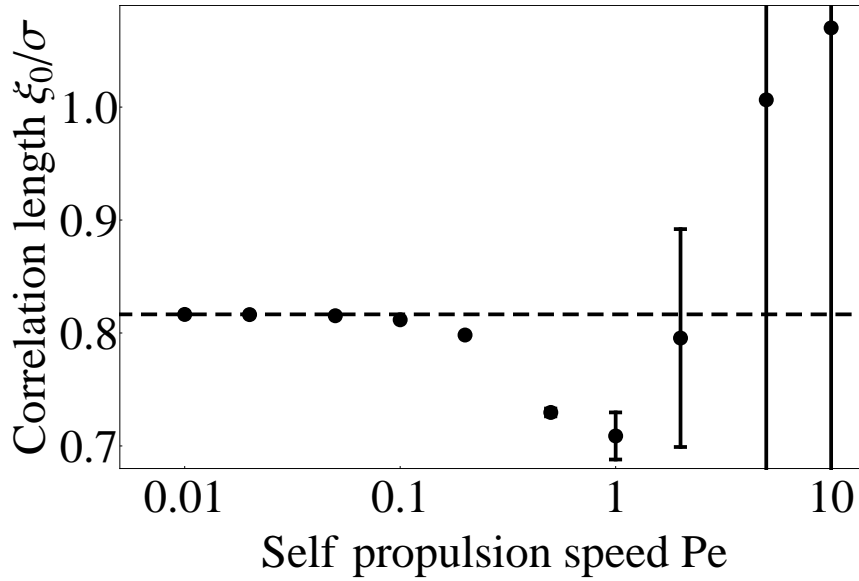


Fig. 5.8 The maximum correlation length ξ_0 is shown in the plot. The dashed line is the analytic value $\xi_0 = \sqrt{2/3}\sigma$ in terms of the particle diameter σ , where a factor $\sqrt{1/3}$ is trivial due to the choice of units. The points are obtained from fitting the analytic function, which we fitted to the data of the F-P equation. For the small self propulsion speeds, there is agreement with the analytic value as well as a small uncertainty.

speeds the correlation length found match the analytic value $\xi_0 = \sqrt{2/3}\sigma \approx 0.816497\sigma$. At the lowest self propulsion speeds, $Pe = 0.01$, the best correlation length is found $\xi_0^{Pe=0.01} = 0.81643(11)\sigma$. At larger self propulsion speeds we see the errors and uncertainties increase. This increase was expected, since we already saw in Figure 5.7 problems with the fit at larger self propulsion speeds.

5.4 Liquid-Gas Phase Coexistence in 2D

In this section we describe the results concerning the usual liquid-gas coexistence in 2 dimensions. We assumed a planar geometry and periodic boundary conditions in the x direction, i.e. $\psi(x, y, \theta) = \psi(x, \theta) = \psi(x + L, \theta)$. We started in an inhomogeneous system, with a low-density part and a high-density part separated by an interface normal to the x direction. Using the F-P equation 2.8 we let the system evolve to a steady state. The obtained low density we call the gas density and the obtained high density we call the liquid density. We confirmed the obtained densities were independent of the initial density profile, as long as a steady state was obtained.

The resulting gas and liquid densities are show in Figure 5.9. In these calculations we used the second virial coefficient given by $b \approx \pi\sigma^2/2$ and the attraction potential given

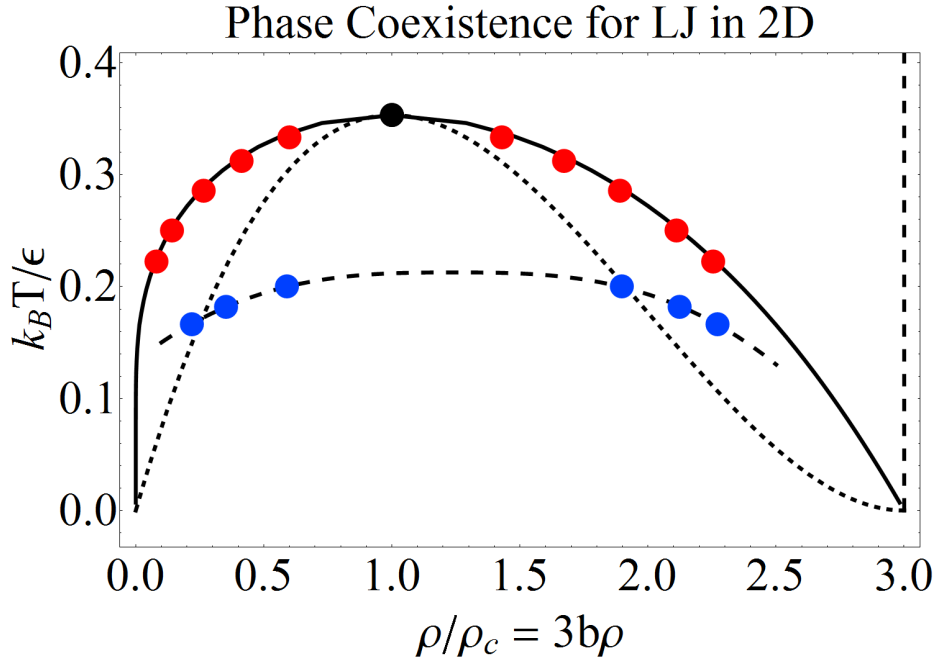


Fig. 5.9 In this figure the obtained gas and liquid densities are shown. The red points are obtained from density profiles in equilibrium with $Pe = 0$ and the blue points at a self propulsion speed $Pe = 1$. The black solid line is obtained from minimizing the free energy, that is exact in the Van der Waals theory. The dotted lines are the spinodal densities obtained from the stability analysis in equilibrium. The black point is the analytically obtained critical temperature and critical density. The dashed vertical line at $\rho/\rho_c = 3$ is the maximum density allowed; otherwise the excluded volume becomes larger than the volume available. The dashed line through the blue points is a guide to the eye.

by the negative part of the usual 6-12 Lennard-Jones potential $\Phi_{12}(r) = \min[0, \Phi_{12}^{LJ}(r)]$. We did not include any correlations $g^{(2)} \equiv 1$, such that at $Pe = 0$ the theory should (and actually does) coincide with minimum free energy results of a Van der Waals gas. In equilibrium we find agreement between the minimization of the free energy and the results from the F-P equation. We did not expect to find agreement between the critical values found and literature values of a Lennard-Jones fluid as obtained from simulations. A Lennard-Jones system in 2 dimensions has a critical point at $(3b\rho_c, T/\epsilon) = (1.67, 0.515)^3$ [5]. However, we have applied an excluded volume approximation to the repulsions in the Lennard-Jones potential. Therefore we do not expect agreement with an exact Lennard-Jones fluid.

³Equivalently $\rho_c \sigma^2 = 0.355$.

Out of equilibrium we find a reduction of the critical temperature. We described in Section 1.2 the two features of active particles regarding phase coexistence. The first feature is the reduction of the critical temperature, because the active particles rip the liquid apart (recall Figure 1.1). The individual particles have by their self-propulsion additional energy, which can be viewed as an effective increase in temperature. The second feature is a new phase coexistence called MIPS (recall Figure 1.2). Therefore an increase in critical temperature could occur. However, this increased critical temperature is not observed nor was it expected. This feature requires the colliding of particles, where the particles point to each other, which requires an orientation-dependent correlation function $g^{(2)}(r, \theta_1, \theta_2)$. However, we used $g^{(2)} \equiv 1$.

Chapter 6

Conclusion

6.1 The Correlation Lengths is not Universal

The most surprising conclusion we found is that the correlation length is not universal. We found the correlation length for particles with low nonzero self propulsion speeds. The correlation length corresponding to the density decay of particles near a wall is $\xi = \sqrt{1/3}\sigma$ in terms of the particle diameter σ . The factor $\sqrt{1/3}$ is trivial due to the chosen units. The correlation length corresponding to the two-particle correlation function (in the zero density limit) is $\xi_0 = \sqrt{2/3}\sigma$. These two correlation lengths deviate by a factor $\sqrt{2}$. When there is no self propulsion, we find an amplitude that is zero and the correlation lengths are no longer defined at vanishing density.

In equilibrium the correlation length is universal, as was showed by applying a pole analysis to the Ornstein Zernike relation [6]. They use the OZ relation, which is different from the approach used in this thesis. This thesis uses the F-P equation. The comparison of the deviation in equilibrium and at low self propulsion speeds, is therefore not straightforward and is beyond the scope of this thesis. One fundamental difference is that in equilibrium the corresponding amplitude is a function of density, while out of equilibrium we only consider the zero density limit and the amplitude is a function of the self propulsion speed.

For a brief explanation of the origin of the factor $\sqrt{2}$, we consider the simplified F-P equations in 2 dimensions for $g^{(2)}$ and $\psi^{(1)}$, respectively

$$\begin{aligned} 0 &= (\nabla_{\mathbf{r}_1}^2 + \nabla_{\mathbf{r}_2}^2 + \partial_{\theta_1}^2 + \partial_{\theta_2}^2) g_{\text{Pe}}^{(2)}(\mathbf{r}_1, \mathbf{r}_2, \theta_1, \theta_2) \\ &= (2\nabla_{\mathbf{r}_{12}}^2 + \partial_{\theta_1} + \partial_{\theta_2}) \left[R_0^{g_{\text{Pe}}^{(2)}}(r_{12}) + R_1^{g_{\text{Pe}}^{(2)}}(r_{12})(\cos \tilde{\theta}_1 - \cos \tilde{\theta}_2) + \text{h.o.} \right], \end{aligned} \quad (6.1a)$$

$$0 = (\nabla_{\mathbf{r}}^2 + \partial_{\theta}^2) \psi_{\text{Pe}}^{(1)}(\mathbf{r}, \theta), = (\nabla_{\mathbf{r}}^2 + \partial_{\theta}^2) \left[R_0^{\psi_{\text{Pe}}^{(1)}}(x) + R_0^{\psi_{\text{Pe}}^{(1)}}(x) \cos \theta + \text{h.o.} \right], \quad (6.1b)$$

where $\tilde{\theta}_{1,2} = \theta_{1,2} - \phi$ denotes the relative angle with ϕ the angular coordinate of \mathbf{r}_{12} . Further, r_{12} is the absolute distance and x is the distance to the wall. When we solve these equations and neglect the higher order terms we get the factor $\sqrt{2}$. For a full explanation we should consider the full derivation which started with Equations 2.8 and 2.10.

6.2 Proof of Concept to find Phase Separation

We have confidence in our methods, since results obtained from different approaches agree. Our obtained correlation function agrees with simulations. We obtained the correct density binodal in equilibrium for a Van der Waals gas. For small self propulsion speeds, the numerical correlation lengths obtained agree with the analytic prediction.

Our method using the F-P equation has advantages and disadvantages. Our method gives more accurate results in the behavior of the density distribution than measuring the result of simulations. At the zero density limit, the obtained correlation function is far more accurate than simulations and it is possible to determine the asymptotic decay.

Motility Induced Phase Separation

Our stability analysis shows that an orientation-dependent correlation function is required to find MIPS. The approach we suggest is similar to finding the normal gas-liquid phase separation. We tried to find MIPS, but we were unsuccessful.

Chapter 7

Outlook

This thesis provides both answers and new questions; more research is required. In Section 7.1 we describe questions we think answers can be given using the current approach with the F-P equation. In Section 7.2 we describe questions for which we think another approach is required.

7.1 With the F-P approach

MIPS

Numerically we were not able to find MIPS.

We used a torque free isotropic WCA potential in 2 dimensions. We considered this entire potential as the short ranged part; the long ranged part of the potential was zero. The potential contributed thus to an excluded volume and corrections since $g^{(2)}$ is not isotropic. We used the equation for the density (Equation 2.8) and assumed a planar geometry. We used a time evaluation to obtain a steady state. We closed this equation by using the low density correlation function, i.e. $g^{(2)} = g^{(2)}(r_{12}, \tilde{\theta}_1, \tilde{\theta}_2)$ with $\tilde{\theta}_{1,2}$ the relative orientations, see Equation 2.11. Our initial density distribution consisted of a high density phase and low density phase, but was orientation independent. We think that by choosing an orientation-dependent density distribution in the interface we would have had a better chance to obtain MIPS. This starting distribution is closer to the distribution that we expect to contain MIPS, and we expect a lower diffusion of the high density phase at the start.

We found MIPS in a quasi 1-dimensional (unphysical) system, where we stated that we could project the gradients $\nabla_{r_{12}} \rightarrow \partial_{x_{12}}$ and introduce a quasi one dimensional force $\int dy g^{(2)} F(\|x_{12}, y\|) \rightarrow g^{(2)} F_{\text{quasi 1D}}(x_{12})$. Also we think we found MIPS in 2

dimensions when we introduced some increase of 20% to 100% to the effective force due to anisotropy of $g^{(2)}$. This increase did not have any physical justification. We made our calculations for relatively low Peclet numbers, $Pe = 1, 2, 5, 10, 20$, otherwise we experienced numerical instabilities. In simulations, larger Peclet numbers $Pe \sim 50$ are required to find MIPS. However, if we assume the zero density correlation function, there is a stronger orientation dependence. So we expect lower self propulsion speeds required for MIPS.

Torques

In our equations of motion we allowed torques. However, during the derivation we assumed the absence of torques for reasons of simplicity, i.e. simplified some equations and our expected phase diagram. We think that torques can be included analytically without much effort, but numerically we expect stability problems.

Correlation Lengths at Large Self Propulsion Speeds

We have doubts about the correlation lengths obtained for the two-body correlation function at large self propulsion speeds. At small self-propulsions speeds, we are confident that the series in self propulsion speeds converges. At large self-propulsion speed we are doubtful about this convergence, because there is a strong coupling between the modes. Furthermore, the numerically obtained data do not correspond with the analytic shape (Equation 5.1). More research should determine whether the model should be different or whether the numerical evaluation of the differential equations gave problems.

7.2 Different Approaches Required

3 Dimensions

In this thesis we mostly do 2-dimensional calculations, because in 3 dimensions additional degrees of freedom make the calculations harder. We can make calculations, however, of the density distribution of an ideal gas (near a wall) in 3 dimensions. Other 3-dimensional calculations are computationally expensive.

There is also another problem: We are uncertain if it is allowed to neglect the momentum of the fluid in 3 dimensions. Possibly, the full hydrodynamic equations should be included. However, we simplified the solvent to only Brownian forces. In

a 2-dimensional geometry, for example a 3 dimensional fluid between two walls, the momentum of the solvent leaks away into the walls and the momentum can therefore be neglected. Without the walls the momentum of the solvent should be taken into account.

Correlation functions at non zero densities

We were not able to determine the correlation functions at nonzero densities. We do not think this can be done with the F-P equation, since an additional integral for the three particle correlations should be evaluated in the differential equation for $g^{(2)}$. This evaluation is computationally too expensive. Perhaps a different approach like OZ can be helpful.

The Correlation Length

The correlation length appears not to be universal when there is a low self propulsion speed, in contrast to equilibrium. It would be interesting to research the difference in the correlation length between this thesis and [6]. Then we would be able to explain where this difference comes from.

This page has been intentionally left blank

References

- [1] Bogoliubov, N. N. (1946). Kinetic equations. *Journal of Physics USSR*, 10(3):265–274.
- [2] Brenner, S. and Scott, R. (2007). *The Mathematical Theory of Finite Element Methods (Texts in Applied Mathematics)*. Springer.
- [3] Clisby, N. and McCoy, B. M. (2006). Ninth and tenth order virial coefficients for hard spheres in d dimensions. *Journal of Statistical Physics*, 122(1):15–57.
- [4] COMSOL (n.d.). Detailed explanation of the finite element method (fem). <https://www.comsol.com/multiphysics/finite-element-method>.
- [5] Costigliola, L., Schröder, T. B., and Dyre, J. C. (2016). Communication: Studies of the lennard-jones fluid in 2, 3, and 4 dimensions highlight the need for a liquid-state $1/d$ expansion. *The Journal of Chemical Physics*, 144(23):231101.
- [6] de Carvalho, R. L. and Evans, R. (1994). The decay of correlations in ionic fluids. *Molecular Physics*, 83(4):619–654.
- [7] Lekner, J. (1982). Parametric solution of the van der waals liquid–vapor coexistence curve. *American Journal of Physics*, 50(2):161–163.
- [8] Paliwal, S. (2017). Data simulations. Not published.
- [9] Pavliotis, G. and Stuart, A. (2008). *Multiscale Methods: Averaging and Homogenization*. Texts in Applied Mathematics. Springer New York.
- [10] Press, W. H., Flannery, B. P., Teukolsky, S. A., and Vetterling, W. T. (1992). *Numerical Recipes in Fortran 77: The Art of Scientific Computing*. Cambridge University Press.
- [11] Prymidis, V., Paliwal, S., Dijkstra, M., and Filion, L. (2016). Vapour-liquid coexistence of an active lennard-jones fluid. *The Journal of Chemical Physics*, 145(12):124904.
- [12] Redner, G. S., Baskaran, A., and Hagan, M. F. (2013). Reentrant phase behavior in active colloids with attraction. *Phys. Rev. E*, 88:012305.
- [13] Solon, A. P., Fily, Y., Baskaran, A., Cates, M. E., Kafri, Y., Kardar, M., and Tailleur, J. (2015). Pressure is not a state function for generic active fluids. *Nature Physics*, 11(8):673–678.

- [14] van Roij, R. (2010). Soft condensed matter theory. Lecture Notes.
- [15] Weeks, J. D., Chandler, D., and Andersen, H. C. (1971). Role of repulsive forces in determining the equilibrium structure of simple liquids. *The Journal of Chemical Physics*, 54(12):5237–5247.

Appendix A

Derivations to obtain the Fokker-Planck Equation

A.1 The Fokker-Planck Equation

In this section we will argue how a stochastic differential equation (SDE) can be written as a partial differential equation (PDE). For most proofs we will refer to the book by Pavliotis and Stuart [9]. We denote the phase space, the initial phase space, the gradient with respect to this phase space and the equations of motion (Equation 2.2) by

$$\mathbf{z}(t) = \{\mathbf{r}_i(t), \boldsymbol{\theta}_i(t)\}_{i \leq N}, \quad (\text{A.1a})$$

$$\mathbf{z}_0 = \mathbf{z}(t_0) = \{\mathbf{r}_i(t_0), \boldsymbol{\theta}_i(t_0)\}_{i \leq N}, \quad (\text{A.1b})$$

$$\nabla_{\mathbf{z}} = \{\nabla_{\mathbf{r}_i}, \nabla_{\boldsymbol{\theta}_i}\}_{i \leq N}, \quad (\text{A.1c})$$

$$\frac{d\mathbf{z}_j}{dt} = \mathbf{h}_j(\mathbf{z}) + \boldsymbol{\gamma}_j(\mathbf{z}) \frac{d\mathbf{W}_j}{dt}. \quad (\text{A.1d})$$

In our class of EOMs the vector $\boldsymbol{\gamma}(\mathbf{z}) = \boldsymbol{\gamma}$ is a constant vector and is independent of the current phase space. All components in this vector are equal to $\sqrt{2}$, i.e. $\boldsymbol{\gamma}_j = \boldsymbol{\gamma} = \sqrt{2}$. The term $\frac{d\mathbf{W}_j}{dt}$ represents Gaussian white noise. So $\boldsymbol{\gamma}_j \frac{d\mathbf{W}_j}{dt}$ contributes in our example only for the rotational and translational Brownian forces. All non-Brownian forces are considered in the term $\mathbf{h}(\mathbf{z})$; this term is named the drift.

Analogue to [9, Ch. 6.1] we note that this process only exists as a distribution and the precise interpretation is an integral equation for $z(t) \in C(\mathbb{R}, \mathbb{Z}^{N \times \tilde{D}})$ with \tilde{D} the

number of degrees of freedom per particle:

$$\mathbf{z}(t) = \mathbf{z}_0 + \underbrace{\int_0^t \mathbf{h}(\mathbf{z}(s)) ds}_{\text{Drift}} + \underbrace{\gamma \int_0^t d\mathbf{W}(s)}_{\text{Diffusion}}. \quad (\text{A.2})$$

We work with the Itô interpretation¹ as defined in [9, Ch. 3].

In [9, Ch. 6.2, 6.3] the existence, uniqueness and the resulting Fokker-Planck equation are proven, which results in the F-P equation for the N -particle density distribution $\psi^{[N]}(\mathbf{z}, t)$:

$$\frac{\partial \psi^{[N]}(\mathbf{z}, t)}{\partial t} = \mathcal{L}^* \psi^{[N]}(\mathbf{z}, t) = -\nabla_{\mathbf{z}} \cdot (\mathbf{h}(\mathbf{z}) \psi^{[N]}(\mathbf{z}, t)) + \nabla_{\mathbf{z}}^2 \psi^{[N]}(\mathbf{z}, t), \quad (\text{A.3})$$

$$\psi^{[N]}(\mathbf{z}, t_0) = \psi_0^{[N]}(\mathbf{z}), \quad (\text{A.4})$$

where $\psi_0^{[N]}$ is some initial distribution function.

A.2 The Reduced Phase Space of the Fokker-Planck Equation

In this section, we will reduce the phase space of the PDE for $\psi^{(N)}(\mathbf{r}^N, \boldsymbol{\theta}^N, t)$, similar to the Bogoliubov-Born-Green-Kirkwood-Yvon hierarchy (BBGKY hierarchy) [1]. The difference is that we have orientation dependencies, but we do not have momentum conservation.

Define a reduced phase space distribution function $\psi^{(n)}(\mathbf{r}^n, \boldsymbol{\theta}^n, t)$, which is the probability of finding n particles at positions \mathbf{r}^n with orientation $\boldsymbol{\theta}^n$ at time t . This distribution function is defined as some permutation factor multiplied by the integral over all possible configurations with n particles at given positions and $N - n$ particles at arbitrary positions. The equation is given by

$$\begin{aligned} \psi^{(n)}(\mathbf{r}^n, \boldsymbol{\theta}^n, t) &= \frac{N!}{(N-n)!} \iint d\mathbf{r}^{N-n} d\boldsymbol{\theta}^{N-n} \psi^{[N]}(\mathbf{r}^N, \boldsymbol{\theta}^N, t) \\ &\equiv \int_{\mathbf{r}, \boldsymbol{\theta}}^{N-n} \psi^{[N]}(\mathbf{r}^N, \boldsymbol{\theta}^N, t), \end{aligned} \quad (\text{A.5})$$

where we denoted for notational purposes $d\mathbf{r}^{N-n} = d\mathbf{r}_{n+1} \dots d\mathbf{r}_N$, $d\boldsymbol{\theta}^{N-n} = d\boldsymbol{\theta}_{n+1} \dots d\boldsymbol{\theta}_N$ and $\int_{\mathbf{r}, \boldsymbol{\theta}}^{N-n} = \frac{N!}{(N-n)!} \iint d\mathbf{r}^{N-n} d\boldsymbol{\theta}^{N-n}$. We separate the ideal part in the (angular) velocity

¹The Stratonovich interpretation will be the same since γ is a constant vector independent of the phase space.

from the two-body interactions:

$$\mathbf{v}_j = \mathbf{v}_j^{\text{id}} + \sum_{i=1}^N \mathbf{F}_{ij}(\mathbf{r}_{ij}, \boldsymbol{\theta}_i, \boldsymbol{\theta}_j), \quad \boldsymbol{\omega}_j = \boldsymbol{\omega}_j^{\text{id}} + \sum_{i=1}^N \boldsymbol{\Gamma}_{ij}(\mathbf{r}_{ij}, \boldsymbol{\theta}_i, \boldsymbol{\theta}_j), \quad (\text{A.6})$$

where the ideal terms $\mathbf{v}_j^{\text{id}} = \sqrt{3}\text{Pe} \mathbf{e}(\boldsymbol{\theta}_j) + \mathbf{F}^{\text{ext}}(\mathbf{r}_j, \boldsymbol{\theta}_j)$ and $\boldsymbol{\omega}_j^{\text{id}} = \boldsymbol{\Gamma}^{\text{ext}}(\mathbf{r}_j, \boldsymbol{\theta}_j)$ only depend on the position and orientation of the particle itself. Then the Fokker-Planck equation (Equation 2.3) can be written as

$$\begin{aligned} & \partial_t \psi^{[N]} + \sum_{j=1}^N \nabla_{\mathbf{r}_j} \cdot [(\mathbf{v}_j^{\text{id}} - \nabla_{\mathbf{r}_j}) \psi^{[N]}] + \sum_{j=1}^N \nabla_{\boldsymbol{\theta}_j} \cdot [(\boldsymbol{\omega}_j^{\text{id}} - \nabla_{\boldsymbol{\theta}_j}) \psi^{[N]}] \\ &= - \sum_{j=1}^N \nabla_{\mathbf{r}_j} \cdot \left[\sum_{i=1}^N \mathbf{F}_{ij} \psi^{[N]} \right] - \sum_{j=1}^N \nabla_{\boldsymbol{\theta}_j} \cdot \left[\sum_{i=1}^N \boldsymbol{\Gamma}_{ij} \psi^{[N]} \right]. \end{aligned} \quad (\text{A.7})$$

where we no longer explicitly write down all dependencies. Now integrate $N - n$ particles out of the equation and multiply by the permutation factor, applying $\int_{\mathbf{r}, \boldsymbol{\theta}}^{N-n} := \frac{N!}{(N-n)!} \iint d\mathbf{r}^{N-n} d\boldsymbol{\theta}^{N-n}$ to the equation. Split the sums up into $1 \leq j \leq n$ and $n < j \leq N$ and we obtain

$$\begin{aligned} & \int_{\mathbf{r}, \boldsymbol{\theta}}^{N-n} \left\{ \partial_t \psi^{[N]} + \sum_{j=1}^n \nabla_{\mathbf{r}_j} \cdot [(\mathbf{v}_j^{\text{id}} - \nabla_{\mathbf{r}_j}) \psi^{[N]}] + \sum_{j=1}^n \nabla_{\boldsymbol{\theta}_j} \cdot [(\boldsymbol{\omega}_j^{\text{id}} - \nabla_{\boldsymbol{\theta}_j}) \psi^{[N]}] \right\} \\ &+ \underbrace{\int_{\mathbf{r}, \boldsymbol{\theta}}^{N-n} \left\{ \sum_{j=n+1}^N \nabla_{\mathbf{r}_j} \cdot [(\mathbf{v}_j^{\text{id}} - \nabla_{\mathbf{r}_j}) \psi^{[N]}] + \sum_{j=n+1}^N \nabla_{\boldsymbol{\theta}_j} \cdot [(\boldsymbol{\omega}_j^{\text{id}} - \nabla_{\boldsymbol{\theta}_j}) \psi^{[N]}] \right\}}_{=0} \\ &= \int_{\mathbf{r}, \boldsymbol{\theta}}^{N-n} \left\{ - \sum_{j=1}^n \nabla_{\mathbf{r}_j} \cdot \left[\sum_{i=1}^n \mathbf{F}_{ij} \psi^{[N]} \right] - \sum_{j=1}^n \nabla_{\boldsymbol{\theta}_j} \cdot \left[\sum_{i=1}^n \boldsymbol{\Gamma}_{ij} \psi^{[N]} \right] \right\} \\ &+ \int_{\mathbf{r}, \boldsymbol{\theta}}^{N-n} \left\{ - \sum_{j=1}^n \nabla_{\mathbf{r}_j} \cdot \left[\sum_{i=n+1}^N \mathbf{F}_{ij} \psi^{[N]} \right] - \sum_{j=1}^n \nabla_{\boldsymbol{\theta}_j} \cdot \left[\sum_{i=n+1}^N \boldsymbol{\Gamma}_{ij} \psi^{[N]} \right] \right\} \\ &+ \underbrace{\int_{\mathbf{r}, \boldsymbol{\theta}}^{N-n} \left\{ - \sum_{j=n+1}^N \nabla_{\mathbf{r}_j} \cdot \left[\sum_{i=1}^N \mathbf{F}_{ij} \psi^{[N]} \right] - \sum_{j=n+1}^N \nabla_{\boldsymbol{\theta}_j} \cdot \left[\sum_{i=1}^N \boldsymbol{\Gamma}_{ij} \psi^{[N]} \right] \right\}}_{=0}. \end{aligned} \quad (\text{A.8})$$

The second and fifth lines each contain an integral of the divergence of a function, which is the integral over the boundary of the function, which equals zero. In the first and third line, all the $N - n$ integrals only depend on $\psi^{[N]}$, so the definition of $\psi^{(n)}$ appears. In the fourth line, $N - n - 1$ integrals only depend on $\psi^{[N]}$, so the definition of $\psi^{(n+1)}$ appears $N - n$ times, up to an exchange of particles. Under the assumptions of identical classical particles, this exchange is trivial. Substitute back the definition of

$\mathbf{v}_j^{\text{id}} = \sqrt{3} \text{Pe} \mathbf{e}(\boldsymbol{\theta}_i) + \mathbf{F}^{\text{ext}}(\mathbf{r}_i, \boldsymbol{\theta}_i)$ and $\boldsymbol{\omega}_j^{\text{id}} = \boldsymbol{\Gamma}^{\text{ext}}(\mathbf{r}_j, \boldsymbol{\theta}_j)$ to obtain

$$\begin{aligned} \frac{\partial \psi^{(n)}}{\partial t} = & - \sum_{j=1}^n \nabla_{\mathbf{r}_j} \cdot \left[\left(\sqrt{3} \text{Pe} \mathbf{e}(\boldsymbol{\theta}_j) \psi^{(n)} + \mathbf{F}^{\text{ext}} \psi^{(n)} + \sum_{i=1}^n \mathbf{F}_{ij} - \nabla_{\mathbf{r}_j} \right) \psi^{(n)} \right] \quad (\text{A.9}) \\ & - \sum_{j=1}^n \nabla_{\boldsymbol{\theta}_j} \cdot \left[\left(\boldsymbol{\Gamma}^{\text{ext}} \psi^{(n)} + \sum_{i=1}^n \boldsymbol{\Gamma}_{ij} - \nabla_{\boldsymbol{\theta}_j} \right) \psi^{(n)} \right] \\ & - \sum_{j=1}^n \nabla_{\mathbf{r}_j} \cdot \iint d\mathbf{r}_{n+1} d\boldsymbol{\theta}_{n+1} \left[\mathbf{F}_{j,n+1} \psi^{(n+1)} \right] \\ & - \sum_{j=1}^n \nabla_{\boldsymbol{\theta}_j} \cdot \iint d\mathbf{r}_{n+1} d\boldsymbol{\theta}_{n+1} \left[\boldsymbol{\Gamma}_{j,n+1} \psi^{(n+1)} \right]. \end{aligned}$$

A.3 Van der Waals Free Energy to the Fokker-Planck Equation in Equilibrium

In this section a different approach is used to obtain the Fokker-Planck equation for a passive Van der Waals gas. So we can compare the results and argue our derivations have the correct limit. The Helmholtz free energy $F(N, V, T)$ is given by $F = U - TS$ with $U(S, V, N)$ the internal energy, T the temperature and S the entropy. Recall the Helmholtz free energy per unit of volume for a homogeneous (constant density) Van der Waals gas $f_{VdW} = \frac{F_{VdW}}{V} = \rho k_B T \left(\log \frac{\rho \Lambda^D}{1 - b\rho} - 1 \right) - a\rho^2$, in D dimensions in equilibrium. Here $\Lambda = \hbar \sqrt{\frac{2\pi}{mk_B T}}$ is the Debye length, $a = - \int d\mathbf{r} \Phi^{\text{long}}(r)/2$ contributes for the attractions between particles and b contributes for the (short ranged) repulsions. The short ranged repulsions can be interpreted as an excluded volume, where $b = B_2^{HS}$ the second Virial coefficient for hard spheres with diameter σ_{HS} .

In density functional theory (DFT), systems with a non-homogeneous density can be considered. Start with the Helmholtz Free Energy functional $\mathcal{F}[\rho]$ where we include an excluded volume contribution. Our density distribution $\rho(\mathbf{r}_1)$ depends on the position \mathbf{r}_1 with equilibrium density distribution $\rho(\mathbf{r}_1)$. From this we will derive the Fokker-Planck equation without self propulsions and interactions up to² the 2nd virial coefficient in the two-body correlation function. In units of $k_B T$ it is given by

$$\mathcal{F}[\rho] = \int d\mathbf{r} \rho(\mathbf{r}) \left(\log \frac{\rho(\mathbf{r}) \Lambda^D}{1 - \rho(\mathbf{r}) b} - 1 \right) - \int d\mathbf{r} d\mathbf{r}_2 K[\Phi^{\text{long}}(\mathbf{r}_2 - \mathbf{r})] \frac{\rho(\mathbf{r}) \rho(\mathbf{r}_2)}{2}. \quad (\text{A.10})$$

²Higher order corrections are not exact within the Van der Waals theory since the approximation $B_n^{HS}/(B_2^{HS})^{n-1} \approx 1$ for all $n > 2$ is made

Here K is a function that only depends on the long ranged part of the pair potential Φ^{long} (often attractions). In the Van der Waals theory we assume no correlations and we have $K'[\Phi^{\text{long}}] = 1$. We take first a functional derivative to $\rho(\mathbf{r})$ and then the spatial gradient ∇ , which gives

$$\frac{\delta\mathcal{F}[\rho]}{\delta\rho(\mathbf{r}_1)} = \log \frac{\rho(\mathbf{r}_1)\Lambda^D}{1 - \rho(\mathbf{r}_1)b} + \frac{b\rho(\mathbf{r}_1)}{1 - \rho(\mathbf{r}_1)b} - \int d\mathbf{r}_2 K[\Phi^{\text{long}}(\mathbf{r}_1, \mathbf{r}_2)]\rho(\mathbf{r}_2), \quad (\text{A.11})$$

$$\nabla_{\mathbf{r}_1} \left(\frac{\delta\mathcal{F}[\rho]}{\delta\rho(\mathbf{r}_1)} \right) = \frac{1}{\rho(\mathbf{r}_1)} \frac{\nabla_{\mathbf{r}_1}\rho(\mathbf{r}_1)}{(1 - b\rho(\mathbf{r}_1))^2} - \int d\mathbf{r}_2 \left(\mathbf{F}_{1,2}^{\text{long}}(\mathbf{r}_2 - \mathbf{r}_1) K'[\Phi^{\text{long}}] \right) \rho(\mathbf{r}_2). \quad (\text{A.12})$$

When K is chosen such that the two-body correlation function $g^{(2)} = K'$ (at distances larger than the size of the excluded volume), the last term can be interpreted as the internal force per unit density.

On the other hand we know $\nabla \left(\frac{\delta\mathcal{F}[\rho]}{\delta\rho(\mathbf{r}_1)} \right)_{\rho_0(\mathbf{r})} = \nabla (\mu - V^{\text{ext}}(\mathbf{r}_1)) = \mathbf{F}^{\text{ext}}$ at equilibrium density $\rho_0(\mathbf{r})$. We notice that in this notation \mathbf{F}^{ext} and \mathbf{F}^{int} are forces per unit density, so we need to multiply by $\rho_0(\mathbf{r})$ to obtain a total force acted on a position. We take the position derivative to obtain the Fokker-Planck equation for a passive system and we notice that this equilibrium result is also a steady state, so $\partial_t \rho_0 = 0$. Thus, we obtain

$$\partial_t \rho_0(\mathbf{r}_1) = 0 = \nabla_{\mathbf{r}_1} \cdot \left[\mathbf{F}^{\text{ext}} \rho_0(\mathbf{r}_1) + \int d\mathbf{r}_2 \mathbf{F}_{1,2}^{\text{long}} \rho_0^{(2)}(\mathbf{r}_1, \mathbf{r}_2) - \frac{\nabla \rho_0(\mathbf{r}_1)}{(1 - b\rho_0(\mathbf{r}_1))^2} \right], \quad (\text{A.13})$$

where $\rho_0^{(2)}(\mathbf{r}_1, \mathbf{r}_2) = \rho_0(\mathbf{r}_1)\rho_0(\mathbf{r}_2)g^{(2)}$. This result holds in equilibrium, with the orientation independent density $\rho_0(\mathbf{r}_1) = \int d\boldsymbol{\theta}_1 \psi(\mathbf{r}_1, \boldsymbol{\theta}_1)$.

In the mean field approximation (or Van der Waals approximation), $K' = g^{(2)} \equiv 1$, so $K[\Phi^{\text{long}}] = \Phi^{\text{long}}$. In the low density approximation (second Virial) $K' = g^{(2)} \equiv \exp[-\beta\Phi^{\text{long}}]$, so $K = \exp[-\beta\Phi^{\text{long}}] - 1$ is the Mayer function.

A.4 The Fokker-Planck and the Excluded Volume Contribution for the Density

In this section, we will derive a more convenient expression for $\iint d\mathbf{r}_2 d\boldsymbol{\theta}_2 \mathbf{F}_{12}^{\text{short}} \psi^{(2)}$ with $\mathbf{F}_{12} = \mathbf{F}_{12}^{\text{short}} + \mathbf{F}_{12}^{\text{long}}$ (part of Equation 2.7), although we have to make some approximations. We will end up with an excluded volume contribution which is accurate to second order in $b\rho$. In Appendix A.3, Equation A.13 the equilibrium result is given for comparison.

We assume that the short ranged potential Φ^{short} has a well defined force leading to some excluded volume. We define the excluded volume as $V^{\text{excl}} = 2b = \int d\mathbf{r} f(\mathbf{r})$ with $f(\mathbf{r}_{12}) = \exp[-\Phi^{\text{short}}(\mathbf{r}_{12})] - 1$ the Mayer function, as in equilibrium Van der Waals theory. We define the pair correlation function $g^{(2)}$ and $u^{(2)}$ with the equilibrium second virial result scaled out, as

$$\psi^{(2)}(1, 2, t) = \psi^{(1)}(1, t)\psi^{(1)}(2, t)g^{(2)}(1, 2, t), \quad (\text{A.14a})$$

$$g^{(2)}(1, 2, t) = \exp[-\beta\Phi^{\text{short}}(\mathbf{r}_{12})] u^{(2)}, \quad (\text{A.14b})$$

$$u^{(2)} = u^{(2)}(1, 2, t), \quad (\text{A.14c})$$

where an argument (i) is shorthand notation for $(\mathbf{r}_i, \boldsymbol{\theta}_i)$. Further, we notice $u^{(2)} \equiv 1$ in the low density limit in equilibrium. Using basic calculus we find

$$\begin{aligned} & \iint d\mathbf{r}_2 d\boldsymbol{\theta}_2 \left[\mathbf{F}_{12}^{\text{short}}(1, 2)\psi^{(2)}(1, 2, t) \right] \quad (\text{A.15}) \\ &= \psi^{(1)}(1, t) \iint d\mathbf{r}_2 d\boldsymbol{\theta}_2 \left[[\nabla_{\mathbf{r}_{12}} f(|\mathbf{r}_{12}|)] \times \left(\psi^{(1)}(2, t)(1 + u^{(2)}(1, 2, t) - 1) \right) \right] \\ &= \psi^{(1)}(1, t) \iint d\mathbf{r}_2 d\boldsymbol{\theta}_2 \left[[\nabla_{\mathbf{r}_{12}} f(|\mathbf{r}_{12}|)] \times \right. \\ & \quad \left. \left(\psi^{(1)}(\mathbf{r}_1, \boldsymbol{\theta}_2, t) + \mathbf{r}_{12} \nabla_{\mathbf{r}_1} \psi^{(1)}(\mathbf{r}_1, \boldsymbol{\theta}_2, t) + \cancel{O(\mathbf{r}_{12})^2} + \psi^{(1)}(2, t)(u^{(2)}(1, 2, t) - 1) \right) \right], \end{aligned}$$

where we made for the term $\psi^{(1)}(2, t) = \psi^{(1)}(\mathbf{r}_2, \boldsymbol{\theta}_2, t)$ a first order approximation in \mathbf{r}_2 near \mathbf{r}_1 , which is allowed under assumptions that the short ranged interactions act on a distance shorter then the density fluctuations (i.e. the thickness of a gas-liquid interface) and is always allowed in the bulk³ of the system. Use partial integration and

³Homogeneous density, no external forces etc.

coordinate changes to obtain

$$\begin{aligned}
&= \psi^{(1)}(1, t) \int d\boldsymbol{\theta}_2 \left\{ \left(\psi^{(1)}(\mathbf{r}_1, \boldsymbol{\theta}_2, t) \underbrace{\int d\mathbf{r}_2 \nabla_{\mathbf{r}_{12}} f(|\mathbf{r}_{12}|)}_{\rightarrow 0} \right) \right. \\
&\quad + \left(\left[\nabla_{\mathbf{r}_1} \psi^{(1)}(\mathbf{r}_1, \boldsymbol{\theta}_2, t) \right] \underbrace{\int d\mathbf{r}_2 \mathbf{r}_{12} \nabla_{\mathbf{r}_{12}} f(|\mathbf{r}_{12}|)}_{\rightarrow 2b} \right) \\
&\quad \left. + \int d\mathbf{r}_2 \psi^{(1)}(\mathbf{r}_2, \boldsymbol{\theta}_2, t) (u^{(2)}(1, 2, t) - 1) \nabla_{\mathbf{r}_{12}} f(|\mathbf{r}_{12}|) \right\} \\
&= \psi^{(1)}(1, t) \int d\boldsymbol{\theta}_2 \left\{ 2b \nabla_{\mathbf{r}_1} \psi^{(1)}(\mathbf{r}_1, \boldsymbol{\theta}_2, t) - \int_{B(\mathbf{r}_1, \sigma_{HS})} d\mathbf{r}_2 \nabla_{\mathbf{r}_{12}} \left(\psi^{(1)}(2, t) (u^{(2)}(1, 2, t) - 1) \right) \right\},
\end{aligned} \tag{A.16}$$

where $B(\mathbf{r}_1, \sigma_{HS})$ is a sphere with center \mathbf{r}_1 , and σ_{HS} is the radius of the short ranged interactions (associated to an equivalent hard core).

In the case we can locally separate variables, i.e. we can split the distance and orientation dependence as⁴ $\psi^{(1)}(\mathbf{r}_1, \boldsymbol{\theta}_2, t) = \psi_r^{(1)}(\mathbf{r}_1, t) \times \psi_\theta^{(1)}(\boldsymbol{\theta}_2, t)$, we obtain

$$\begin{aligned}
&- \iint d\mathbf{r}_2 d\boldsymbol{\theta}_2 \left[\mathbf{F}_{12}^{\text{short}}(1, 2) \psi^{(2)}(1, 2, t) \right] \\
&= -2b\rho \left[\nabla_{\mathbf{r}_1} \psi^{(1)}(1, t) \right] - \psi^{(1)}(1, t) \int d\boldsymbol{\theta}_2 \int_{B(\mathbf{r}_1, \sigma_{HS})} d\mathbf{r}_2 \nabla_{\mathbf{r}_{12}} \left(\psi^{(1)}(2, t) (u^{(2)}(1, 2, t) - 1) \right) \\
&= \underbrace{\frac{\nabla_{\mathbf{r}_1} \psi^{(1)}(1, t)}{(1 - b\rho(1, t))^2}}_{\text{Eff. enhanced diffusion}} - \underbrace{\nabla_{\mathbf{r}_1} \psi^{(1)}(1, t)}_{\text{Normal diffusion}} + \cancel{O((b\rho(1, t))^2 \nabla_{\mathbf{r}_1} \psi^{(1)}(1, t))} \\
&\quad - \psi^{(1)}(1, t) \int d\boldsymbol{\theta}_2 \int_{B(\mathbf{r}_1, \sigma_{HS})} d\mathbf{r}_2 \nabla_{\mathbf{r}_{12}} \left(\psi^{(1)}(2, t) (u^{(2)}(1, 2, t) - 1) \right)
\end{aligned} \tag{A.17}$$

with $\rho(1, t) = \rho(\mathbf{r}_1, t) = \int d\boldsymbol{\theta} \psi^{(1)}(\mathbf{r}_1, \boldsymbol{\theta}, t)$ the local density. We find an effective enhancement in the diffusion due to the repulsions. If $u^{(2)}$ is anisotropic, we also find an effective force.

We neglected cubic terms in $b\rho$. Even in equilibrium, higher order terms in $b\rho$ will not agree in general. In the Van der Waals approximation, the Virial coefficient B_n are assumed to be powers of the second Virial coefficients $B_n = B_2^{n-1}$ for $n > 2$. Even in the case of hard spheres in equilibrium, this approximation is not exact, see Table A.1.

⁴I assume this approximation is valid locally in a neighborhood for each \mathbf{r} . It is valid if there is locally translational invariance and the size of the particle is much smaller than the size of an interface.

	B_3/B_2^2	B_4/B_2^3	B_5/B_2^4	B_6/B_2^5	B_7/B_2^6	B_8/B_2^7
2D	0.782	0.532	0.333	0.199	0.115	0.065
3D	0.625	0.287	0.110	0.038	0.013	0.004

Table A.1 An overview of higher Virial coefficients of hard spheres in terms of the second Virial coefficient. The coefficient are taken from [3].

A.5 Translational Invariance in the Two Body Correlation Function

In this section we will impose the local density approximation to obtain a Fokker-Planck Equation for the two-body correlation function $g^{(2)}$. We will start with the expression for $\psi^{(n)}$ in Equation 2.6, with $n = 2$. We will use a local density approximation and we will assume we can neglect external forces and external torques and we have translational and rotational invariance.

We start with a torque free, external field free system, i.e.

$$\begin{aligned}
\frac{\partial \psi^{(2)}}{\partial t} &= - \sum_{j=1}^2 \nabla_{\mathbf{r}_j} \cdot \left[\sqrt{3} \text{Pe} \mathbf{e}(\boldsymbol{\theta}_j) \psi^{(2)} + \sum_{i=1}^2 \mathbf{F}_{ij} \psi^{(2)} - \nabla_{\mathbf{r}_j} \psi^{(2)} \right] \\
&\quad - \sum_{j=1}^2 \nabla_{\boldsymbol{\theta}_j} \cdot \left[-\nabla_{\boldsymbol{\theta}_j} \psi^{(2)} \right] - \sum_{j=1}^2 \nabla_{\mathbf{r}_j} \cdot \left[\iint d\mathbf{r}_3 d\boldsymbol{\theta}_3 \mathbf{F}_{j,3} \psi^{(3)} \right] \\
&= - \nabla_{\mathbf{r}_1} \cdot \left[\sqrt{3} \text{Pe} \mathbf{e}(\boldsymbol{\theta}_1) \psi^{(2)} - \mathbf{F}_{12} \psi^{(2)} - \nabla_{\mathbf{r}_1} \psi^{(2)} + \iint d\mathbf{r}_3 d\boldsymbol{\theta}_3 \mathbf{F}_{13} \psi^{(3)} \right] \\
&\quad - \nabla_{\mathbf{r}_2} \cdot \left[\sqrt{3} \text{Pe} \mathbf{e}(\boldsymbol{\theta}_2) \psi^{(2)} - \mathbf{F}_{21} \psi^{(2)} - \nabla_{\mathbf{r}_2} \psi^{(2)} + \iint d\mathbf{r}_3 d\boldsymbol{\theta}_3 \mathbf{F}_{23} \psi^{(3)} \right] \\
&\quad + \nabla_{\boldsymbol{\theta}_1}^2 \psi^{(2)} + \nabla_{\boldsymbol{\theta}_2}^2 \psi^{(2)},
\end{aligned} \tag{A.18}$$

where $\psi^{(2)} = \psi^{(2)}(1, 2, t) = \psi^{(2)}(\mathbf{r}_1, \boldsymbol{\theta}_1, \mathbf{r}_2, \boldsymbol{\theta}_2, t)$. Impose translational invariance to obtain $\psi^{(2)}(\mathbf{r}_{12}, \boldsymbol{\theta}_1, \boldsymbol{\theta}_2, t)$ only dependent on the distance of the two particles $\mathbf{r}_{12} = \mathbf{r}_2 - \mathbf{r}_1$, but not on the absolute position:

$$\begin{aligned}
\frac{\partial \psi^{(2)}}{\partial t} &= - \nabla_{\mathbf{r}_{12}} \cdot \left[\sqrt{3} \text{Pe} (\mathbf{e}(\boldsymbol{\theta}_2) - \mathbf{e}(\boldsymbol{\theta}_1)) \psi^{(2)} + 2\mathbf{F}_{12} \psi^{(2)} - 2\nabla_{\mathbf{r}_{12}} \psi^{(2)} \right] \\
&\quad + \iint d\mathbf{r}_3 d\boldsymbol{\theta}_3 (\mathbf{F}_{23} - \mathbf{F}_{13}) \psi^{(3)} \Big] + \nabla_{\boldsymbol{\theta}_1}^2 \psi^{(2)} + \nabla_{\boldsymbol{\theta}_2}^2 \psi^{(2)}.
\end{aligned} \tag{A.19}$$

Use the definition of the two-body correlation function $g^{(2)}$ in the local density approximation, i.e.

$$\psi^{(2)}(\mathbf{r}_{12}, \boldsymbol{\theta}_1, \boldsymbol{\theta}_2) = \psi^{(1)} \psi^{(1)} g^{(2)}(\mathbf{r}_{12}, \boldsymbol{\theta}_1, \boldsymbol{\theta}_2), \quad (\text{A.20})$$

where $\psi^{(1)}$ is locally constant, to obtain

$$\begin{aligned} \frac{\partial g^{(2)}}{\partial t} = & -\boldsymbol{\nabla}_{\mathbf{r}_{12}} \cdot \left[\sqrt{3} \text{Pe} (\mathbf{e}(\boldsymbol{\theta}_2) - \mathbf{e}(\boldsymbol{\theta}_1)) g^{(2)} + 2\mathbf{F}_{12} g^{(2)} - 2\boldsymbol{\nabla}_{\mathbf{r}_{12}} g^{(2)} \right. \\ & \left. + \iint d\mathbf{r}_3 d\boldsymbol{\theta}_3 (\mathbf{F}_{23} - \mathbf{F}_{13}) \frac{\psi^{(3)}}{(\psi^{(1)})^2} \right] + \boldsymbol{\nabla}_{\boldsymbol{\theta}_1}^2 g^{(2)} + \boldsymbol{\nabla}_{\boldsymbol{\theta}_2}^2 g^{(2)}. \end{aligned} \quad (\text{A.21})$$

A.6 Rotational Invariance in 2D at Low Densities

In this section, the Fokker-Planck Equation for $g^{(2)}$ is further derived. Start with Equation A.21 in the low density limit where the inequality $\psi^{(3)} \ll (\psi^{(1)})^2$ holds. The two-body force can be written as the gradient of the corresponding potential:

$$\begin{aligned} \frac{\partial g^{(2)}}{\partial t} = & -\boldsymbol{\nabla}_{\mathbf{r}_{12}} \cdot \left[\sqrt{3} \text{Pe} (\mathbf{e}(\boldsymbol{\theta}_2) - \mathbf{e}(\boldsymbol{\theta}_1)) g^{(2)} - 2(\boldsymbol{\nabla}_{\mathbf{r}_{12}} \Phi_{12}) g^{(2)} - 2\boldsymbol{\nabla}_{\mathbf{r}_{12}} g^{(2)} \right] \\ & + \boldsymbol{\nabla}_{\boldsymbol{\theta}_1}^2 g^{(2)} + \boldsymbol{\nabla}_{\boldsymbol{\theta}_2}^2 g^{(2)}. \end{aligned} \quad (\text{A.22})$$

We consider the 2 dimensional case, thus the absolute angles (with respect to the x axis) $\boldsymbol{\theta}_1 = \theta_1$ and $\boldsymbol{\theta}_2 = \theta_2$ are scalars. We introduce polar coordinates in the distance vector (so particle 1 is at the origin), i.e. $\mathbf{r}_{12} = (r, \phi)$ and recall in polar coordinates $\boldsymbol{\nabla}_{\mathbf{r}_{12}} = \left(\hat{\mathbf{r}} \frac{\partial}{\partial r} + \hat{\boldsymbol{\phi}} \frac{1}{r} \frac{\partial}{\partial \phi} \right)$. We use the polar coordinates representation

$$\mathbf{e}(\theta) = \hat{\mathbf{x}} \cos \theta + \hat{\mathbf{y}} \sin \theta = \hat{\mathbf{r}} \cos(\theta - \phi) + \hat{\boldsymbol{\phi}} \sin(\theta - \phi)$$

to find

$$\begin{aligned} \frac{\partial g^{(2)}}{\partial t} = & \partial_{\theta_1}^2 g^{(2)} + \partial_{\theta_2}^2 g^{(2)} - \boldsymbol{\nabla}_{\mathbf{r}_{12}} \cdot \left[\right. \\ & \hat{\mathbf{r}} \left(\sqrt{3} \text{Pe} (\cos(\theta_2 - \phi) - \cos(\theta_1 - \phi)) g^{(2)} - 2(\partial_r \Phi_{12}) g^{(2)} - 2\partial_r g^{(2)} \right) \\ & \left. + \hat{\boldsymbol{\phi}} \left(\sqrt{3} \text{Pe} (\sin(\theta_2 - \phi) - \sin(\theta_1 - \phi)) g^{(2)} + \frac{2}{r} \left(-\partial_\phi \Phi_{12} g^{(2)} \right) - \frac{2}{r} \partial_\phi g^{(2)} \right) \right], \end{aligned} \quad (\text{A.23})$$

where we used $\Phi_{12} = \Phi_{12}(r)$ is independent of ϕ . For any vector \mathbf{A} the divergence is given by $\boldsymbol{\nabla} \cdot \mathbf{A} = \boldsymbol{\nabla} \cdot (\hat{\mathbf{r}} A_r + \hat{\boldsymbol{\phi}} A_\phi) = \frac{1}{r} \frac{\partial(r A_r)}{\partial r} + \frac{1}{r} \frac{\partial A_\phi}{\partial \phi}$ in polar coordinates. We apply

this rule and we obtain

$$\begin{aligned} \frac{\partial g^{(2)}}{\partial t} &= \partial_{\theta_1}^2 g^{(2)} + \partial_{\theta_2}^2 g^{(2)} \\ &- \left[\frac{1}{r} \frac{\partial}{\partial r} \left(r \left(\sqrt{3} \text{Pe} (\cos(\theta_2 - \phi) - \cos(\theta_1 - \phi)) g^{(2)} - 2 (\partial_r \Phi_{12}) g^{(2)} - 2 \partial_r g^{(2)} \right) \right) \right. \\ &\left. + \frac{1}{r} \frac{\partial}{\partial \phi} \left(\sqrt{3} \text{Pe} (\sin(\theta_2 - \phi) - \sin(\theta_1 - \phi)) g^{(2)} - 2 \frac{1}{r} \partial_\phi g^{(2)} \right) \right]. \end{aligned} \quad (\text{A.24})$$

With straightforward algebra we get

$$\begin{aligned} \frac{\partial g^{(2)}}{\partial t} &= \partial_{\theta_1}^2 g^{(2)} + \partial_{\theta_2}^2 g^{(2)} - \left[\frac{1}{r} \left(-2 (\partial_r \Phi_{12}) g^{(2)} - 2 \partial_r g^{(2)} \right) \right. \\ &\left. + \frac{\partial}{\partial r} \left(\sqrt{3} \text{Pe} (\cos(\theta_2 - \phi) - \cos(\theta_1 - \phi)) g^{(2)} - 2 (\partial_r \Phi_{12}) g^{(2)} - 2 \partial_r g^{(2)} \right) \right] \\ &- \frac{1}{r} \left(\sqrt{3} \text{Pe} (\sin(\theta_2 - \phi) - \sin(\theta_1 - \phi)) \partial_\phi g^{(2)} - 2 \frac{1}{r} \partial_\phi^2 g^{(2)} \right). \end{aligned} \quad (\text{A.25})$$

We impose rotation invariance in the correlation function, so the correlation function only depends on the relative orientation, but not on the absolute orientation $g^{(2)}(r, \phi, \theta_1, \theta_2) = g^{(2)}(r, \theta_1 - \phi, \theta_2 - \phi)$ and $\partial_\phi g^{(2)} = -\partial_{\theta_1} g^{(2)} - \partial_{\theta_2} g^{(2)}$. It is now possible to introduce relative orientation $\theta_1 - \phi \rightarrow \theta_1$ and $\theta_2 - \phi \rightarrow \theta_2$:

$$\begin{aligned} \frac{\partial g^{(2)}}{\partial t} &= \partial_{\theta_1}^2 g^{(2)} + \partial_{\theta_2}^2 g^{(2)} - \left[\frac{1}{r} \left(-2 (\partial_r \Phi_{12}) g^{(2)} - 2 \partial_r g^{(2)} \right) \right. \\ &\left. + \frac{\partial}{\partial r} \left(\sqrt{3} \text{Pe} (\cos \theta_2 - \cos \theta_1) g^{(2)} - 2 (\partial_r \Phi_{12}) g^{(2)} - 2 \partial_r g^{(2)} \right) \right] \\ &+ \left(\frac{\sqrt{3} \text{Pe}}{r} (\sin \theta_2 - \sin \theta_1) (\partial_{\theta_1} g^{(2)} + \partial_{\theta_2} g^{(2)}) + \frac{2}{r^2} (\partial_{\theta_1} + \partial_{\theta_2})^2 g^{(2)} \right). \end{aligned} \quad (\text{A.26})$$

We use this equation to determine the pair correlation function in the low-density limit numerically.

Appendix B

Numerics

The numerical evaluations of partial differential equations are a major part of this thesis. Programs exist that can do this evaluation where the user only needs limited knowledge about the numerics. These programs can be used as a black box; a PDE and settings are inserted in the program and the program returns numerical data. One of these programs is COMSOL[®]. The goal of this appendix is to give a very brief introduction to the methods this program uses.

A boundary value problem is a (partial) differential equation with boundary conditions on all boundaries; the F-P equation for most steady state systems are often boundary problems. In contrast, initial value problem have some boundaries with no restrictions. An example is a system that is known at time t_0 , but not at time t_1 ; there are no restrictions on time t_1 .

B.1 Finite Element Methods

The goal of this section is to introduce the finite element method (FEM) and to give the reader an intuitive idea what happens. This method computes a boundary value problem for partial differential equations. We will not go into detail; we do not show everything is well defined, we do not prove our statements nor will we give error estimates. Books exist about FEMs [2], that hold several chapters to ensure everything is well defined and introduce for instance Sobolev spaces and many different norms. The website of the program COMSOL[®] we use, provides a short introduction as well [4].

Measure

We consider any boundary value problem that has at most a second order derivative, is linear (or linearized) in the unknown function and has at all boundaries some boundary condition. Both the range as well as the domain can be higher dimensional. We examine the 1 dimensional example

$$h(x)\frac{\partial^2 u(x)}{\partial x^2} + i(x)\frac{\partial u(x)}{\partial x} + j(x)u(x) = f(x) \quad \text{in } U \subset \mathbb{R}, \quad (\text{B.1a})$$

$$u(x_0) = u_0 \quad u'(x_N) = u_1 \quad U = (x_0, x_N) \quad (\text{B.1b})$$

where $h(x)$, $i(x)$, $j(x)$ and $f(x)$ arbitrary functions $U \rightarrow \mathbb{R}$ and we assume everything is well defined. We can multiply the PDE with any function $v(x) \in V$ (as long as the resulting formula are well defined¹) and integrate over the domain U . Use partial integration to get rid of second order derivatives² and we can define the relation

$$\begin{aligned} \langle f, v \rangle &\stackrel{\text{def}}{=} \int_U f(x)v(x) \, dx & (\text{B.2}) \\ &= \int_U [h(x)u''(x) + i(x)u'(x) + j(x)u(x)]v(x) \, dx \\ &\stackrel{\text{P.I.}}{=} \int_U [-h'(x)v(x) - h(x)v'(x) + i(x)v(x)]u'(x) \, dx + \int_U j(x)v(x)u(x) \, dx \\ &\quad + h(x)v(x)u'(x)|_{x_0}^{x_N} \stackrel{\text{def}}{=} a(u, v). \end{aligned}$$

The idea behind this method is that the correct $u(x)$ satisfies $\langle f, v \rangle = a(u, v)$ for all $v(x)$. For a finite subset of functions (i.e. continuous piecewise linear on some grid) we state that the best $u_h(x)$ satisfies this equation for all $v_h(x)$ in the same subset of functions. We notice $a(u, v)$ and $\langle f, v \rangle$ are both bilinear in their arguments, so we will formulate this problem as a linear algebra problem.

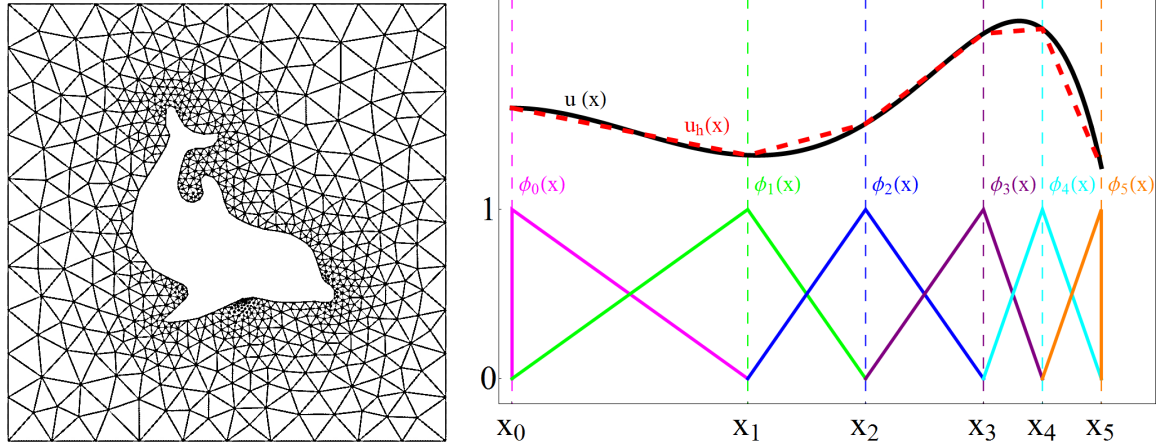
Shape Functions

Now we want to consider a set of shape functions $V_h \subset V$, such that V_h has a finite basis. We take a partition of the domain; which is a set of sub-domains. In Figure B.1a an example of a 2 dimensional partition using a triangularization is given. The mesh is the maximal size of an element in the partition. The words mesh, grid or partition

¹We do not denote nor prove the conditions required to keep everything well defined, (almost) all examples from physics are.

²Motivation: More functions exist with a first (weak) derivative than with a second (weak) derivative.

in this context are often used interchangeably. Next we take the set of continuous³ piecewise polynomial functions up to some order P (or some other shape) as the set of shape functions, such that the functions reduced to a sub-domain are polynomial.



(a) Example of a 2D triangularization. The mesh does not have to be uniform. Image by Hans Petter Langtangen.

(b) Example of a finite basis. A set of basis functions $\{\phi_i(x)\}$ is given (continuous piecewise linear functions) for this grid. Further, $u_h(x)$ is a linear combination of the basis function and is an approximation of $u(x)$.

Fig. B.1 Visual illustrations for finite element method.

In our example we can take the set of piecewise linear functions. In Figure B.1b an example of a basis and a visual representation of a function $u \in V$ that is approximated by a piecewise linear function $u_h \in V_h$ are illustrated.

Linear Algebra

If we define $\{\phi_0, \dots, \phi_n\}$ as the set of basis functions, where we constructed these basis functions to be nonzero in a small number of sub-domains such as the example in Figure B.1b, then we can define

$$A_{ij} = a(\phi_i, \phi_j), \quad F_i = \langle f, \phi_i \rangle, \quad (\text{B.3})$$

where A is a $n \times n$ matrix⁴ and \mathbf{F} a vector with n elements. Since we reduced the PDE to a linear algebra problem, we only have to solve the equation $\mathbf{A}\mathbf{U} = \mathbf{F}$ for the

³For continuous piecewise smooth bounded functions the weak derivative exists.

⁴It is common to choose the basis function to be 1 on one grid point and zero on all other, in other words $\phi_i(x_j) = \delta_{ij}$. This way the matrix A_{ij} is sparse and some of the proofs are simplified.

vector \mathbf{U} . We conclude

$$u_h(x) = \sum_i U_i \phi_i(x), \quad (\text{B.4})$$

which is an approximation of $u(x)$.

Error Estimations

A next step would be to argue that this approximation is the best approximation within V_h , but this is not in the scope of this introduction. Further, there are a priori and posteriori estimates for the errors $\|u - u_h\|_*$ under different norms, which are a function of the mesh and order of the polynomials used. In fact, it is possible to estimate local errors and refine the mesh where the error is the worst. By refining the mesh uniformly or non uniformly the error could be reduced. These estimates are given, explained and proven in [2, Ch. 9]. In this thesis it was considered sufficient for the error to be small enough, such that a refined mesh would not give a noticeable difference.

B.2 Initial Value Problem

An initial value problem is a PDE where we know the initial condition but do not know the final state. An example is

$$u'(t) = F[u(t), t] \quad t \in (t_0, t_n), \quad (\text{B.5a})$$

$$u(t_0) = u_0, \quad (\text{B.5b})$$

where $F[u(t), t]$ is some functional. The most simple way to solve this is numerically, is with the Forward Euler method, which states

$$u(t_i) = u(t_{i-1}) + u'(t_{i-1})h_i + O(h_i^2), \quad (\text{B.6})$$

where $h_i = t_i - t_{i-1}$. At step i the error is $O(h_i^2)$, so the total error is $O(h)$ (if $h = h_i$ for all i). There are other methods that converge faster. The fourth-order Runge-Kutta

[10, Ch. 16.1, 16.2] method (RK4) states in 1 dimension that

$$\left\{ \begin{array}{l} u(t_i) = u(t_{i-1}) + \frac{h_i}{6} [k_1 + 2k_2 + 2k_3 + k_4] + O(h_i^5), \\ k_1 = F[u(t_{i-1}), t_{i-1}], \\ k_2 = F\left[u(t_{i-1}) + \frac{h_i}{2}k_1, t_{i-1} + \frac{h_i}{2}\right], \\ k_3 = F\left[u(t_{i-1}) + \frac{h_i}{2}k_2, t_{i-1} + \frac{h_i}{2}\right], \\ k_4 = F[u(t_{i-1}) + h_ik_3, t_i]. \end{array} \right. \quad (\text{B.7})$$

At step i the error is $O(h_i^5)$, so the total error is $O(h^4)$, which converges faster than the Forward Euler method.

This page has been intentionally left blank

Appendix C

Addendum: The Correlation Length Beyond the Low Self Propulsion Speed Limit

This addendum has been added July 4th 2017.

In Section 3.2 we gave an analytic expression for the one particle distribution function for an ideal gas near a (hard) wall. This analytic expression only holds for small Peclet numbers, $Pe < Pe_{\text{crit}}$. We found the correlation length to be $\xi = \sqrt{1/3}\sigma$ with $\sigma = \sqrt{3}x_0$ the particle diameter. We also found the numerical correlation length, which we illustrated in Figure 5.4a, Section 5.1. For the two-body correlation function we illustrated the correlation length in Figure 5.8.

Before, we were only able to make analytical derivations for small Peclet numbers. In this addendum, we will derive an expression beyond the low Peclet number limit for an ideal gas near a wall.

C.1 Analytical Expression for the One Particle Distribution Function away from a Wall

We start with Equation 3.13, which reduces in a planar geometry in 2 dimensions, $\psi^{(1)}(\mathbf{r}, \boldsymbol{\theta}) = \psi^{(1)}(x, \theta)$, near a hard wall to

$$\sqrt{3} Pe \cos \theta \partial_x \psi^{(1)} = \partial_x^2 \psi^{(1)} + \partial_\theta^2 \psi^{(1)}. \quad (\text{C.1})$$

We substitute $\psi^{(1)}(x, \theta)|_{x \gg X_{\text{Pe}}} = \exp[-x/\xi]B(\theta)$ for asymptotic large values of $x \gg X_{\text{Pe}}$, where $B(\theta)$ is some 2π periodic function and ξ the correlation length to be determined. In contrast to Section 3.2, we do not make a Fourier expansion in $B(\theta)$. We obtain

$$0 = B''(\theta) + \left[\frac{1}{\xi^2} + \sqrt{3} \text{Pe} \cos \theta \frac{1}{\xi} \right] B(\theta), \quad (\text{C.2})$$

which is solved by the Mathieu¹ sine $S(a, q, \theta/2)$ and Mathieu cosine $C(a, q, \theta/2)$ function

$$B(\theta) = c_1 C\left(\frac{4}{\xi^2}, -\frac{2\sqrt{3} \text{Pe}}{\xi}, \frac{\theta}{2}\right) + c_2 S\left(\frac{4}{\xi^2}, -\frac{2\sqrt{3} \text{Pe}}{\xi}, \frac{\theta}{2}\right), \quad (\text{C.3})$$

where c_1 and c_2 are integration constant. We notice that for $0 \neq q = -\frac{2\sqrt{3} \text{Pe}}{\xi}$, only a countable number of solutions is 2π -periodic and even in θ , these satisfy

$$\frac{4}{\xi^2} = a = a_r(q) = a_r\left(-\frac{2\sqrt{3} \text{Pe}}{\xi}\right) \quad (\text{C.4})$$

where² $r/2 \in \mathbb{Z}$ and $a_r(q)$ is the Mathieu Characteristic A function³. Thus we need to solve this equation for ξ for some $r/2 \in \mathbb{Z}$.

This equation has no analytical solutions⁴. For a given r in the limit $\text{Pe} \rightarrow 0$, we find that correlation length equals $\xi_{\text{Pe} \rightarrow 0}(r) = \frac{2}{|r|} \frac{\sigma}{\sqrt{3}}$; in other words, the dominant correlation length is the one corresponding to a smallest $|r|$ with a nonzero amplitude in our solution. The case $r = 0$ does not match the results obtained from the F-P equation. For $r = \pm 2$, the obtained correlation length ξ and orientation dependence $B(\theta)$ match with results obtained from the F-P equation, and thus this ξ is the correlation length.

In summery, the correlation length ξ in terms of x_0 and orientation dependent distribution function $B(\theta)$ satisfy

$$\frac{4}{\xi^2} = a_2 \left(-\frac{2\sqrt{3} \text{Pe}}{\xi} \right), \quad (\text{C.5a})$$

$$B(\theta) = c_1 C\left(\frac{4}{\xi^2}, -\frac{2\sqrt{3} \text{Pe}}{\xi}, \frac{\theta}{2}\right) + c_2 S\left(\frac{4}{\xi^2}, -\frac{2\sqrt{3} \text{Pe}}{\xi}, \frac{\theta}{2}\right), \quad (\text{C.5b})$$

¹See also: E. W. Weisstein, "Mathieu function." From MathWorld—A Wolfram Web Resource. <http://mathworld.wolfram.com/MathieuFunction.html>.

²For $r/ \in \mathbb{Z}$ we obtain 4π -periodic function.

³The odd solutions are obtained by using the Mathieu Characteristic B function.

⁴Although in the limits $\frac{2\sqrt{3} \text{Pe}}{\xi} \ll 1$ or $\frac{4}{\xi^2} \ll 1$ we can approximate $a_r(q)$ to obtain an analytic equation.

where we can find the integration constants c_1 and c_2 by demanding that the result is real valued, $0 = \Im[B(0)] = \Im[B(2\pi)]$, and 2π periodic, $B(0) = B(2\pi)$, and fit to the remaining real-valued amplitude. We do not have to fit to the correlation length nor the orientation dependence shape $\sim B(\theta)$.

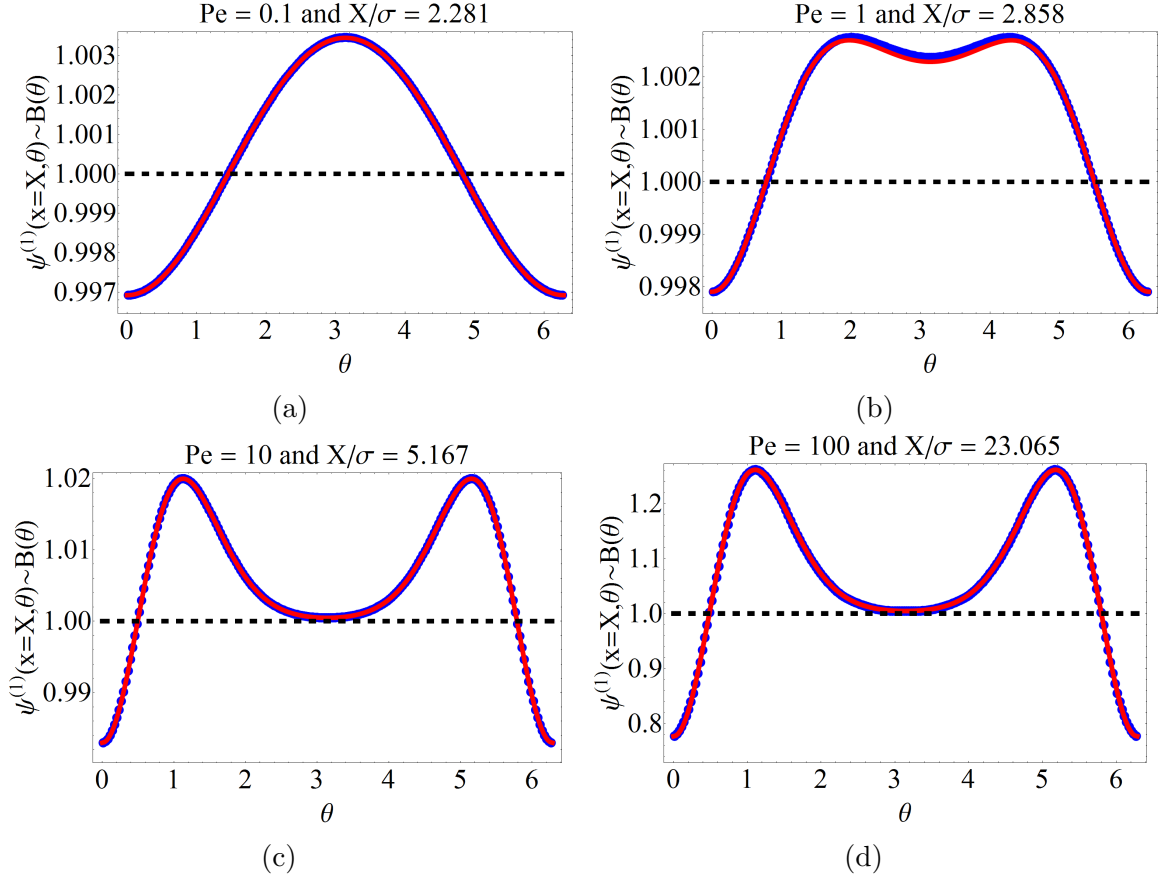


Fig. C.1 In this figure the orientation dependent part is of the one particle distribution function $\psi_{x=X}^{(1)}(\theta) \sim B(\theta)$ of an ideal gas far from a wall, is shown at large distance X for different Peclet numbers. The blue points are obtained from evaluation of the F-P equation, the red line is obtained from the analytic expression.

C.2 The Correlation Length of an Ideal Gas Near a Wall

In this section, we compare the obtained orientation dependent profile $B(\theta)$ and the correlation length in Equation C.5 with those we obtained after fitting to the numerical evaluated F-P equation. In Figure C.1 we see the orientation dependent distribution

$\psi^{(1)}(x = X, \theta)$ at large distance X , which agrees with the result we obtained from $B(\theta)$ (Equation C.5).

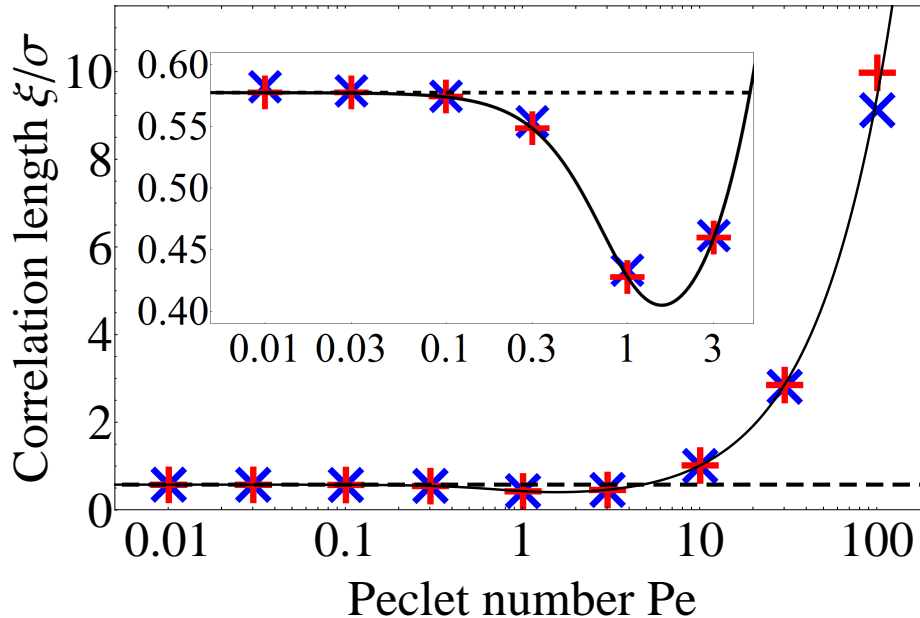


Fig. C.2 The correlation length is shown as a function of Peclet numbers for an ideal gas near a wall. This figure is modified from Figure 5.4a. The main difference is that the correlation length $\xi_{Pe=100}$, obtained from the evaluated F-P equation, was recalculated and an analytical obtained correlation length is included (solid line). We obtained from the evaluated F-P equation the correlation length from both the density (blue crosses \times) as from the polarizations (red plus $+$).

In Figure C.2 the correlation lengths are illustrated. This Figure is a remake of Figure 5.4a. The correlation length $\xi_{Pe=100}$, obtained from the fit to the evaluated F-P equation, was recalculated and we included the analytical obtained correlation length (Equation C.5). We find good agreement between the analytical correlation length and the correlation length obtained from the evaluation of the F-P equation.

C.3 The Correlation Length of the Correlation Function

We have not found an analytical expression for the correlation length of the correlation function. However, we tried $\xi_0 = \sqrt{2}\xi$ as a solution. In Figure C.3 we show the result. This figure is a modified version of Figure 5.8. Even though we do not have an

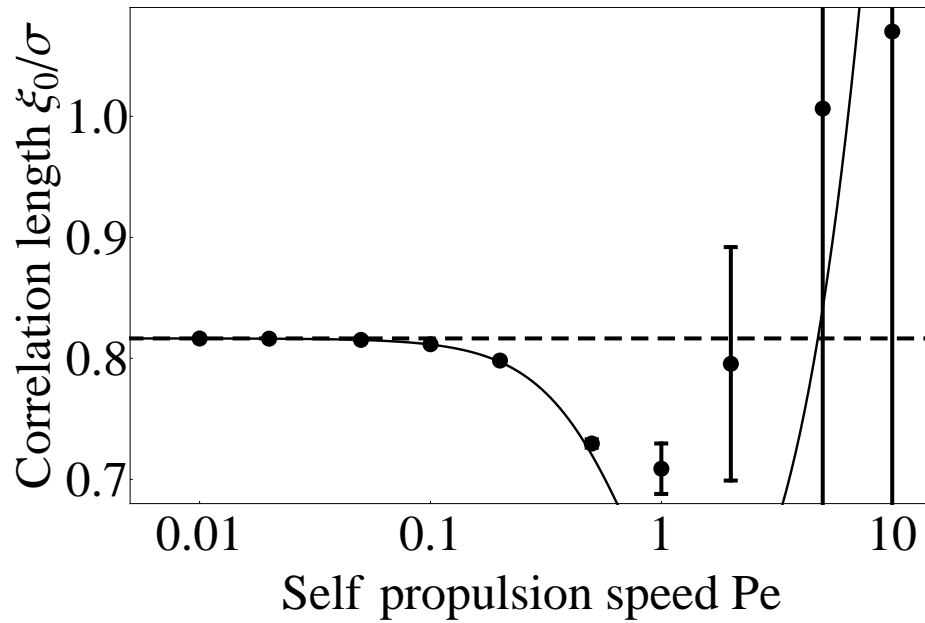


Fig. C.3 The correlation length for the two body distribution function is shown as a function of Peclet numbers. This figure is modified from Figure 5.8. We have included the analytical expression for the correlation length $\xi_0 = \sqrt{2}\xi$ obtained from the ideal gas near a wall (solid line). We don't have any analytical justification for the correlation length of the correlation function beyond the $Pe \rightarrow 0$ limit. The points were obtained from the numerical evaluated F-P equation.

analytical justification, the agreement is surprising for low and medium Peclet numbers. For large Peclet numbers, we have doubts about the points - indicated by the large error bars.

This page has been intentionally left blank